Ultrafast electronic response of Ag(111) and Cu(111) surfaces: From early excitonic transients to saturated image potential

V. M. Silkin

Institute of Physics, P.O. Box 304, Bijenička c. 46, 10000 Zagreb, Croatia;
Departamento de Física de Materiales and Centro Mixto CSIC–UPV/EHU, Facultad de Ciencias Químicas, Universidad del País Vasco,
Apdo. 1072, 20080 San Sebastián, Basque Country, Spain;
Donostia International Physics Center (DIPC), P. de Manuel Lardizabal, 4, 20018 San Sebastián, Basque Country, Spain
and IKERBASQUE, Basque Foundation for Science, 48011, Bilbao, Spain

P. Lazić and N. Došlić

Institute Rudjer Bošković, P.O. Box 180, Bijenička c. 54, 10000 Zagreb, Croatia

H. Petek

Department of Physics and Astronomy and Pittsburgh Quantum Initiative (PQI), University of Pittsburgh,
Pittsburgh, Pennsylvania 15260, USA

B. Gumhalter[*]

Institute of Physics, P.O. Box 304, Bijenička c. 46, 10000 Zagreb, Croatia

We investigate the evolution of attosecond to femtosecond screening and emergent potentials that govern the dynamics and energetics of electrons and holes excited in the various stages of multiphoton photoemission processes and control the photoelectron yield in recently reported experiments [X. Cui, C. Wang, A. Argondizzo, S. Garrett-Roe, B. Gumhalter, and H. Petek, Nat. Phys. **10**, 505 (2014)]. The study is focused on the dynamical screening of holes created in preexistent quasi-two-dimensional Shockley state bands on Ag(111) and Cu(111) surfaces and of electrons excited to the intermediate and emerging screened states. Using the formalism of self-consistent electronic response, we analyze first the effects of screening on the dynamics of photoexcited electrons and holes and then of the Coulomb correlated photoexcited pair. Special attention is paid to the correlated primary electron-hole states, which commence as transient surface excitons and develop in the course of screening into uncorrelated electrons and holes propagating in the image potential and surface state bands, respectively. The obtained results enable to establish a consistent picture of transient electron dynamics at Ag(111) and Cu(111) surfaces that are becoming accessible by the time-, energy-, and momentum-resolved pump-probe multiphoton photoelectron spectroscopies.

PACS number(s): 71.10.−w, 73.20.−r, 78.47.J−, 79.60.−i

I. INTRODUCTION

Screening is a fundamental process that determines the dynamical properties of charged Fermi liquids [1]. Of special interest are the dynamical screening properties of inhomogeneous electron gas and their manifestations in the various measurements, particularly at solid surfaces and interfaces where photoexcited charged particles can turn on Coulomb interactions whose effects can be gleaned from a variety of energy and time-resolved electron spectroscopies.

The act of probing the properties of electronic systems by various spectroscopic techniques involves in one way or another nonadiabatic external perturbations that cause transitions of the system from the initial equilibrium into the ionized or excited final states. These primary transitions give rise to fast deviations from the initial charge density distribution in the system which, in turn, couple to the dynamical polarization or screening response of the surrounding electronic density. This coupling is strong because it is governed by the Coulomb forces throughout the duration of the screening process.

In photoelectron spectroscopies that leave the system in an ionized final state, dynamical screening is essential for achieving the total energy balance and manifests itself through the energy relaxation shifts and characteristic line shapes of the probed electronic states. The effect is particularly strong for localized initial electronic states or orbitals of atoms and molecules in the bulk [2–4] and at surfaces [4,5].

Metals and degenerate semiconductors are the media, which support most efficient screening of external perturbations either in the bulk or at surfaces. The spatial extension of the screening charge induced near the surface by external perturbation fields depends on the density of the electron gas. For metallic densities of practical interest, the major part of the screening charge is localized within a few atomic radii of the surface region, with the induced charge density or Friedel oscillations extending deeper into the bulk [6–13]. It also turns out that for perturbations induced by an external charge spatially restricted outside the equilibrium surface electronic charge density, the self-consistent linear response provides a complete picture of screening which has a classical analog in the form of image charge [6,8,11].

Early theoretical studies of the screening properties of surfaces were focused mainly on the energetic and spatial

*Corresponding author: branko@ifs.hr

aspects of the induced and image charge, which proved accessible by the then available experimental techniques (for review, see Chaps. 2 and 3 in Ref. [11] and references therein). Less attention has been paid to temporal aspects of surface screening because the detection of screening charge formation and saturation requires techniques with high resolution both in the energy and time domains. However, the advent of time- and energy-resolved electron spectroscopies [14–21], and particularly of the multiphoton photoemission (MPPE) spectroscopies utilizing ultrashort laser pulses, has provided tools for studying ultrafast electron dynamics under the strong influence of screening processes, which in metals are manifest on the femto- and attosecond time scale.

One of the most fascinating characteristics of low index surfaces of some metals are the series of quasi-two-dimensional (Q2D) electronic band states in the surface projected bulk band gaps [22,23]. These states arise from the interplay of the truncated periodic crystal potential, which prevents the electrons to move inside the crystal with energies and momenta that span the band gap, and the attractive image potential, which keeps them localized close to the surface. In the standard nomenclature, the lowest surface state or resonance derived from the nearly free-electron sp band is termed the Shockley surface state (SS state with energy E_{SS}), and the unoccupied Rydberg-like states detached from the vacuum level and extending below the upper sp-band gap edge are termed the image potential states (IP states with the lowest state energy E_{IP}). Both groups of states exhibit a quadratic dispersion with effective masses of the order of free electron mass [24–26]. Calculations of the energetics of these states [27] have been based on the assumption of instantaneous image potential $V^{im}(z)$, where z is the electron coordinate perpendicular to the surface. Abundant experimental evidence from steady-state experiments including high-resolution one-photon photoemission (HR 1PPE), inverse photoemission (IPE), continuous wave two-photon photoemission (cw 2PPE), etc., fully supports this picture [24–26,28–33]. The first series of investigations of nonadiabatic aspects of ultrafast dynamics of quasiparticles in surface bands assumed such preexistent SS and IP states [34–41], in accord with the existence of instantaneous (nonretarded) $V^{im}(z)$ modifying the crystal pseudopotential in the surface region.

The assumption of instantaneous $V^{im}(z)$ becomes inapplicable on the ultrashort time scale because surface screening is a dynamical, damped oscillatory process whose cycle duration and attenuation can be in the simple models identified with the inverse of surface plasmon frequency and its width, respectively. Thus, upon sudden promotion of a probe charge in front of the surface, the formation of its stationary image charge and ensuing potential occur after several such cycles when dephasing processes eliminate the screening transients. Only in that limit the employment of standard static $V^{im}(z)$ can be justified. Apart from these energetic aspects, the dynamical screening processes also give rise to specific features in the optical absorption (OA) and photoemission (PE) spectra, which cannot be interpreted within the one-electron picture but require a full many-body approach [2,3,42,43].

The most frequently employed spectroscopic methods for studying the surface electronic structure are based either on the photon-induced emission of electrons out of the initial occupied states into outgoing states above the vacuum level E_V in which they are detected (the case of 1PPE), or on radiative transitions of the injected probe electrons from the states above E_V into unoccupied states below E_V (the case of IPE). In OA, the system remains neutral and the probed states are electron polarization states, either localized or itinerant. The more involved techniques of MPPE and sum frequency generation (SFG) are applied to create coherent sums of pathways in which multiple interactions with photon fields excite electrons from the occupied initial, over the unoccupied intermediate into the final unoccupied states below and above E_V. Here, the information on the amplitudes of intermediate states is contained in the final photoelectron or photon yield, respectively. Since the yields are detected long after the completion of transient surface dynamics, their integrated spectra must satisfy the on-the-energy-shell requirements.

The primary excited states of 1PPE (i.e., prior to screening and relaxation of quasiparticles) are characterized by a single uncompensated charge of the hole localized in the system and of the electron in the delocalized outgoing state above E_V in which interactions with the response of the system are neglected in the so-called sudden approximation [44]. The primary and intermediate states of MPPE and SFG are polarization states comprising the hole evolving from the initial state and electrons excited and relaxing during the sequence of excitations induced by the pump photon field. Here, it is important to observe that before the formation of screening charge the photoexcited electron and hole interact through the bare (unscreened) Coulomb potential, which may bind the pair into a localized excitonic state [45–47] [see Fig. 1(a)]. The duration of such primary excitonic states is largely determined by the time scale of screening, which is system specific. To analyze these processes, we note that at any instant of evolution of the probed system, each excited quasiparticle couples to the electronic response of the environment. This produces a twofold effect on their motion: (i) dynamical screening renormalizes the spectrum of one-particle energies (dynamical self-energy effect) and (ii) the bare Coulomb interaction between the excited electron and hole in OA, MPPE, and SFG at surfaces is strongly reduced during the screening from a monopole-dominated to a much weaker interaction of excited electrons with the dipole composed of the hole and its image. Such a dynamical vertex correction effect has so far been treated only approximately for bulk systems [49–52]. Screening is a complex nonlinear process but a simplification of its description arises at metal surfaces where it can be adequately treated within the self-consistent linear response formalism, i.e., described by the standard density-density response function representable by a boson type of propagator [35–38]. In this case, the primary transient excitonic interaction and both effects (i) and (ii) can be schematically illustrated on the example of single-color 3PPE from an SS-band state as shown in Fig. 1(b).

Therefore, besides the basic one-particle picture of surface electronic excitations, a prerequisite for the interpretation of
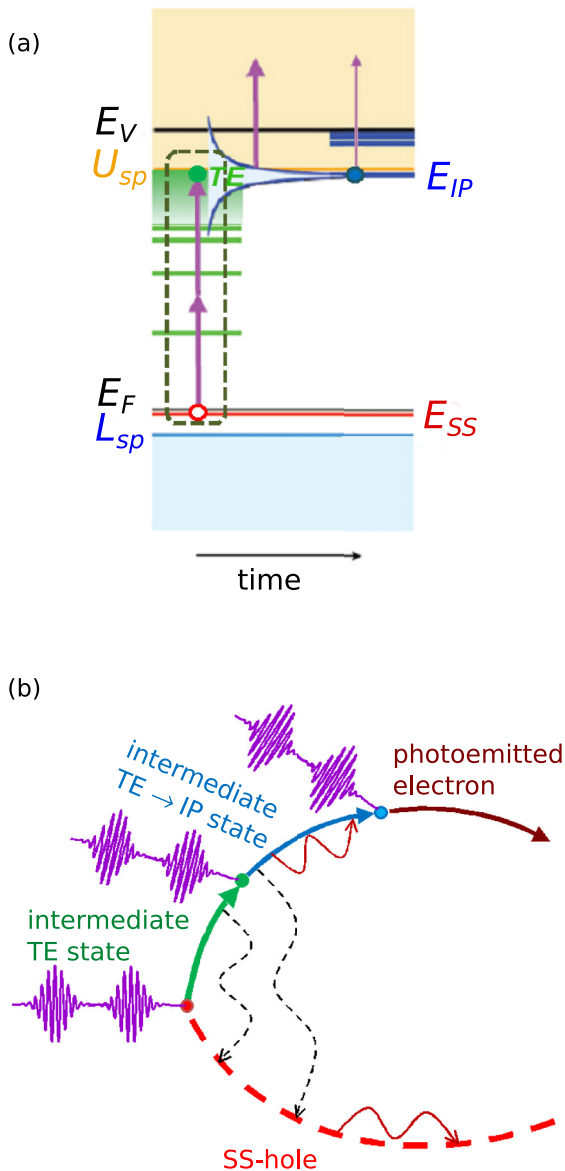
FIG. 1. (Color online) (a) Illustration of the role of transient excitonic states (denoted by horizontal lines enclosed in dashed box) as intermediate states in 3PPE from SS band on Ag(111) surface in the experiment described in Ref. [48]. Optical transitions are induced by two delayed identical phase-locked laser pulses with frequency tuned to two-photon resonance with relaxed IP and SS states, $2\hbar\omega_{pulse} = E_{IP} - E_{SS}$. Electrons excited in high transient excitonic states, which in the model description of Sec. III C make a Rydberg-like quasicontinuum below U_{sp}, converge into the emergent first image potential state as denoted. Dashed rounded box symbolizes coherent e-h pairs constituting the TE wave packet. (b) Diagrammatic illustration of the amplitude of two-pulse photoexcitation processes in (a). Dashed and full lines denote the SS-hole and excited electron propagators, respectively. Dashed wavy lines denote the dynamically screened e-h excitonic interactions, full wavy lines denote the dynamical e-e and h-h interactions involving bosonized electronic charge density fluctuations that give rise to self-energy renormalizations of excited quasiparticles. Open end boson propagators describing excitation of real charge density fluctuations are not shown in the picture. All interactions renormalize the 3PPE amplitude. The time axis is common to both panels.

spectroscopic measurements that probe the system electronic properties on the ultrashort time scale is the knowledge of concurrent evolution of screening. This becomes particularly important in the interpretation of MPPE using ultrashort laser pulses because some of the intermediate steps of perturbative photoemission may proceed via the states created in and affected by ultrafast screening processes. Here the detection and identification of the various manifestations of screening as a paradigm of many-body interactions enables deep insight into the electron dynamics of the studied systems.

In Refs. [12,13,47], we have set the foundations for a theoretical description of the temporal and spatial evolution of the induced screening charge and ensuing potentials, respectively, and applied it to the Cu(111) surface. The latter is considered as a prototype system for demonstrating the existence of well defined SS- and IP-band states on metals, both experimentally and theoretically. In the present paper, we extend the earlier investigations of the screening properties of Cu(111) surface and complement them with the analogous ones for Ag(111). The rationale for this comparative study is that despite the similar energetics of SS and IP states on Ag(111) and Cu(111), these two paradigmatic surfaces exhibit very dissimilar electron polarization dynamics, which can be utilized to demonstrate the different regimes of ultrafast screening at surfaces. In Sec. II, we modify and improve the earlier developed method for calculation of the electronic structure and response properties of thick metallic slabs and use it to derive the ground-state electronic structure and dynamical electronic response of Ag(111) and Cu(111) surfaces. In this approach, the SS-bands are incorporated in the initial electronic structure preexistent with respect to the action of external probe fields that polarize and excite the system. In Sec. III A, we apply the developed response formalism to study the screening dynamics of SS holes created in the primary excitation steps common to 1PPE, MPPE, OA, and SFG. In Sec. III B, we extend our study to the screening of Coulomb interactions between the primary excited electrons and holes and derive their temporal and spatial limits in the region outside the surface. Analogously to the screening of single quasiparticles elaborated in Sec. III A, we find significant difference between the duration of saturation of screening of interparticle interactions on Ag(111) and Cu(111) surfaces. Noninstantaneous saturation of screening allows the formation of transient excitonic states in which the primary excited electron-hole (e-h) pairs are bound by the yet unscreened interparticle interactions. In Sec. III C, we calculate the energy spectra, wave functions, and lateral extensions of transient excitons emerging in primary excitations from occupied SS bands on Ag(111) and Cu(111). In the course of screening, the primary coherent excitonic states evolve into asymptotic uncorrelated IP-SS electron-hole states [53]. The pace of this process is dictated by the dynamics of formation of electron image potential and corresponding IP states on pertinent surfaces, which we investigate in Sec. III D. The concluding section puts the discussed processes within a unified framework that has enabled consistent interpretation of the recent time-resolved 3PPE spectra from surface bands on Ag(111) [48] and Cu(111) [15]. Perspectives of the investigations of the described phenomena in other condensed matter systems are briefly outlined.

II. SELF-CONSISTENT LINEAR ELECTRONIC RESPONSE TO PERTURBATIONS AT SURFACES

Linear electronic response formalism, which we adopt to study the dynamics of screening at (111) surfaces of Cu and Ag, has been elaborated in Sec. 2 of Ref. [38] and here we reiterate only its most salient features. It is based on the calculation of self-consistent retarded linear response function $\chi(\mathbf{r}, \mathbf{r}', t - t')$ in the slab model of the pertinent metal. The slab consisting of several tens of atomic layers is assumed translationally invariant and isotropic in the $(x, y) = \boldsymbol{\rho}$ planes parallel to the slab surface. The z axis is perpendicular to the slab and for convenient positioning of the image potential we take the origin $z = 0$ to coincide with the outermost right-hand-side (RHS) crystal plane (cf. Fig. 1 in Ref. [38]). The effective one-electron potential within the slab is adopted from Ref. [27]. Exploiting the symmetry of the problem, we can introduce the two-dimensional (2D) spatial and time Fourier transform (FT) of the response function $\chi(\boldsymbol{\rho} - \boldsymbol{\rho}', z, z', t)$ for the slab (hereafter $\hbar = 1$ and electron charge $e = -1$):

$$\chi(\mathbf{Q}, z, z', \omega) = \int d^2\bar{\boldsymbol{\rho}} \, e^{-i\mathbf{Q}\bar{\boldsymbol{\rho}}} \int dt \, e^{i\omega t} \chi(\bar{\boldsymbol{\rho}}, z, z', t), \quad (1)$$

where $\bar{\boldsymbol{\rho}} = (\boldsymbol{\rho} - \boldsymbol{\rho}')$ and $\mathbf{Q}$ is a 2D wave vector parallel to the surface. The dimension of the thus defined $\chi(\mathbf{Q}, z, z', \omega)$ is (length)$^{-4} \times$ (energy)$^{-1}$.

The various levels of approximate treatment of screening were discussed in Ref. [54]. Our earlier analyses of the linear electronic response of metal surfaces have shown that the properties of $\chi(\mathbf{Q}, z, z', \omega)$ describing the interactions of probe particles with screening electrons are accurately described in the self-consistent random-phase approximation (SC RPA), which neglects exchange effects in the vertices of Coulomb interactions [55]. On the level of SC RPA the response function (1) is obtained by solving the integral equation

$$\chi(\mathbf{Q}, z, z', \omega) = \chi^0(\mathbf{Q}, z, z', \omega) + \int dz_1 \int dz_2 \chi^0(\mathbf{Q}, z, z_1, \omega)$$
$$\times V(\mathbf{Q}, z_1, z_2) \chi(\mathbf{Q}, z_2, z', \omega). \quad (2)$$

Here, $\chi^0(\mathbf{Q}, z, z', \omega)$ is the retarded response function of noninteracting electron gas in the slab, and

$$V(\mathbf{Q}, z_1, z_2) = V_Q e^{-Q|z_1 - z_2|} = \frac{2\pi}{Q} e^{-Q|z_1 - z_2|} \quad (3)$$

is the 2D FT of the bare Coulomb potential (for details, see Sec. II of Ref. [38]). In the following, we shall find convenient to use the spectral or Lehmann representation of the response function (2), which we write in the form

$$\chi(\mathbf{Q}, z_1, z_2, \omega) = \int_0^\infty d\omega' \tilde{\mathcal{S}}(\mathbf{Q}, z_1, z_2, \omega')$$
$$\times \left(\frac{1}{\omega - \omega' + i\delta} - \frac{1}{\omega + \omega' + i\delta} \right), \quad (4)$$

where δ is a positive infinitesimal. Here, the spectrum of electronic excitations partaking in the response is obtained as

$$\tilde{\mathcal{S}}(\mathbf{Q}, z_1, z_2, \omega) = -(1/\pi) \text{Im} \chi(\mathbf{Q}, z_1, z_2, |\omega|) \text{sign}(\omega), \quad (5)$$

TABLE I. Values of the parameters used in the calculations of the response function (2) and energetics of primary exciton on Ag(111) and Cu(111) surfaces presented in Table II. All energies are in eV and referenced to the vacuum level $E_V = 0$, which is the natural origin for the image potential state energies E_{IP}. E_F is the Fermi level energy and L_{sp}, U_{sp}, E_{SS}, and $E_{\text{IP}}^{(1)}$ denote the energy of the lower and upper edges of the surface projected bulk sp-band gap, surface-state energy, and the first image potential state energy at the $\bar{\Gamma}$ point of the surface Brillouin zone, respectively. m_{SS}^* and m_{IP}^* denote effective masses of the SS hole and IP electron in the lateral (x, y) directions, respectively, in the units of free electron mass. In the present slab model based on the pseudopotentials from Ref. [27], the electron mass in the U_{sp} band and m_{IP} are equal.

surface	E_F	U_{sp}	L_{sp}	$E_{\text{SS}} - E_F$	m_{SS}^*	$E_{\text{IP}}^{(1)}$	m_{IP}^*
Ag(111)	−4.56	−0.66	−4.96	−0.065	0.397 [26]	−0.77	1
Cu(111)	−4.94	−0.69	−5.83	−0.39	0.412 [26]	−0.82	1

and fully characterizes the linear response of electron gas in the slab calculated in the SC RPA. The components of the spectrum (5) are sharp peaks (poles) signifying coherent bulk, surface and multipole plasmon excitations and a quasicontinuum of intraband electron-hole pair excitations. We shall investigate their role in screening processes separately for the quasiparticles excited to and propagating in the *preexistent states* on Ag(111) and Cu(111) surfaces (i.e., the eigenstates of the initial Hamiltonian describing the system prior to the formation of screening charge induced by the excited quasiparticles), and then for the electrons excited into the intermediate states of MPPE or OA emerging and evolving during the screening processes (hereafter termed *emergent states*). This is in contrast to the majority of earlier studies in which only the preexistent states are considered as intermediate states [53,56,57]. The parameters used in the present calculation are listed in Table I.

Current slab model calculations were performed with 31 atomic layers. We first calculate the response function $\chi^0(\mathbf{Q}, z, z', \omega)$ of noninteracting electrons in the eigenstates $\langle \boldsymbol{\rho}, z | \mathbf{K}, n \rangle = \exp(i\mathbf{K}\boldsymbol{\rho})\psi_n(z)/\sqrt{L^2}$ of the slab potential [27] using the expression

$$\chi^0(\mathbf{Q}, z, z', \omega) = \frac{2}{L^2} \sum_{n, n'} \psi_n(z)\psi_{n'}(z)\psi_n(z')\psi_{n'}(z')$$
$$\times \sum_{\mathbf{K}} \frac{f_{\mathbf{K}n} - f_{\mathbf{K}+\mathbf{Q}n'}}{E_{\mathbf{K}n} - E_{\mathbf{K}+\mathbf{Q}n'} + \omega + i\delta}. \quad (6)$$

Here, L is the quantization length along the slab, $\mathbf{K}$ and n are the 2D wave vector and the quantum number describing the motion of slab electrons in the directions parallel and perpendicular to the surface, respectively, the sum over $\mathbf{K}$, n and n' runs over the occupied and unoccupied states, and $f_{\mathbf{K}n}$ is the Fermi occupation factor. In the numerical evaluation of Eq. (6), we adopted the approach proposed by Eguiluz [58,59] and extended it to the case of variable effective masses in Ref. [60]. In order to take into account the screening effects related to the presence of fully occupied d-valence energy bands, we employ the spd model of Liebsch [11,61,62] in which the d-polarizable medium is described by a dielectric
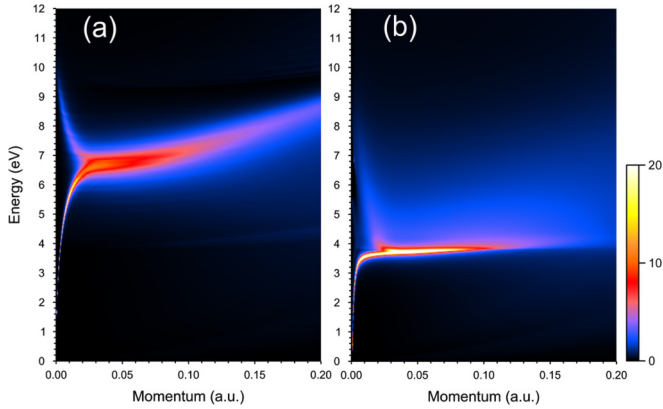
FIG. 2. (Color online) Calculated surface loss function (7) of Ag(111) surface (a) without and (b) with inclusion of the d-polarizable medium. Splitting of the surface plasmon peak [66] and the appearance of hot spots at small values of Q are due to the finite thickness slab effect and discretization of the Q space, respectively.

function extracted from the available measured dielectric functions of Ag and Cu [63,64]. The effect of inclusion of the d-band polarization on the surface response function is demonstrated on the example of surface response function [65] $g(\mathbf{Q},\omega)$ whose imaginary part, termed the loss function, reads

$$-\frac{1}{\pi}\text{Im}g(\mathbf{Q},\omega) = -\frac{1}{\pi}\text{Im}\left[\frac{2\pi}{Q}\int dz_1 \int dz_2 e^{Q(z_1+z_2)}\right.$$
$$\left. \times \chi(\mathbf{Q},z_1,z_2,\omega)\right], \quad (7)$$

and directly measures the coupling of surface electronic excitation spectrum (5) to external probes [see text after Eq. (29) in Sec. III B]. Contour plots of (7) shown in Figs. 2 and 3 clearly demonstrate that taking into account only the sp-like states produces the surface loss function with the surface plasmon peak located around the energy $\hbar\omega_s = 6.7$ eV on Ag(111) surface [Fig. 2(a)] and $\hbar\omega_s = 8.7$ eV on Cu(111) surface [Fig. 3(a)], where ω_s denotes the surface plasmon frequency for $Q = 0$. However, inclusion of the valence
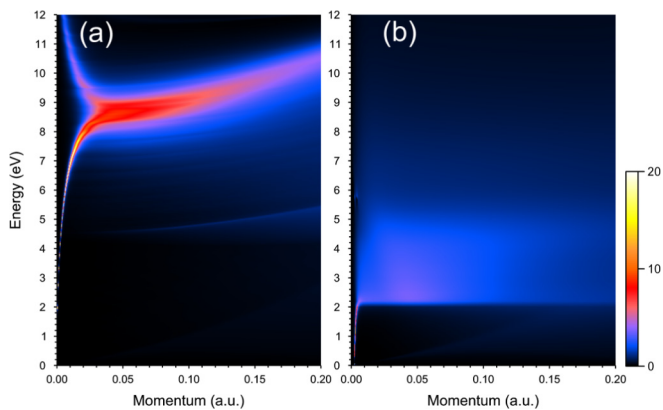

FIG. 3. (Color online) Same as in Fig. 2 but for the Cu(111) surface. In (a), the surface plasmon corresponds to a well defined peak, whereas in (b), this structure is destroyed by the d renormalization.

d-electronic structure into consideration shifts the surface plasmon energy on Ag(111) downward to 3.7 eV [Fig. 2(b)], in close agreement with experiments [67,68]. On the other hand, the d-electronic medium produces a notably more dramatic effect on the electronic excitation spectra of Cu(111) surface. In this case, as seen in Fig. 3(b), the surface plasmon ceases to exist as a well defined coherent excitation.

III. SCREENING IN SURFACE EXCITATION PROCESSES

A. Ultrafast screening of quasiparticles in preexistent states

In OA, 1PPE and the first stage of MPPE spectroscopy of solids holes are created in preexistent states. Hence, in the studies of interactions of the hole charge density with primary excited electrons, it is convenient to solve first the problem of hole motion in the preexistent state basis [so-called Kohn-Luttinger ansatz [69] (KLA)]. In the context of the present discussion this means to solve for the motion of a suddenly created band state hole whose uncompensated charge is then subjected to interaction with the electronic response of the environment described by (2). This problem was solved in Ref. [41] by resorting to cumulant approach developed earlier [36] to calculate the various propagators or single-particle amplitudes $G_i(t)$ of electrons and holes constituting the expressions for more complex 1PPE, MPPE, and OA amplitudes [39–41,70,71]. These propagators provide relevant information on the ultrafast dynamics of quasiparticles at time t after their promotion into the preexistent states $|i\rangle$ in surface bands at the instant t_0 [36–38]. In the present slab model, $|i\rangle = |\mathbf{K},n\rangle$ denotes the initial quasiparticle state in the nth 2D band with the momentum $\mathbf{K}$ and total energy $E_i = E_{\mathbf{K},n}$. Taking $t_0 = 0$, we have the shorthand notation

$$G_i(t) = G_i^0(t)\exp[C_i(t)], \quad (8)$$

where $G_i^0(t) = \exp(\mp iE_it)\theta(t)$ is the single-particle propagator describing the unperturbed motion of the electron (sign $-$) and hole (sign $+$) injected into the formerly unoccupied (occupied) band state $|i\rangle$ with unperturbed energy E_i. The cumulant $C_i(t)$ is given by

$$C_i(t) = -\int_{-\infty}^{\infty}\rho_i(\nu)\frac{1 - i\nu t - e^{-i\nu t}}{\nu^2}d\nu, \quad (9)$$

where $\rho_i(\nu)$ is the cumulant joint spectral density of excitations of the quasiparticle and the system response [41]. $\rho_i(\nu)$ can to a good approximation be modelled by the second-order term $\rho_i^{(2)}(\nu)$, which leads to the quasiparticle energy shifts and decay rates consistent with the image potential and Fermi golden rule (FGR), respectively. For calculational convenience we shall assume that $\rho_i(\nu)$ is bounded from above and below, i.e., that all its moments are finite. A detailed description of the calculation of $\rho_i^{(2)}(\nu) = \rho_{\mathbf{K},n}^{(2)}(\nu)$ from the quasiparticle energies $E_{\mathbf{K},n}$ and the spectral density of the surface response function (4) relevant to the present problem was presented in Sec. III of Ref. [38] and Sec. 4 of Ref. [41].

To demonstrate the steady-state limit of the quasiparticle amplitude (8), we explore the long-time stationary behavior of

the partial derivative:

$$\frac{\partial C_i(t)}{\partial t} = i \int_{-\infty}^{\infty} \rho_i(\nu) \frac{1 - \cos \nu t}{\nu} d\nu - \int_{-\infty}^{\infty} \rho_i(\nu) \frac{\sin \nu t}{\nu} d\nu. \tag{10}$$

The first integral on the RHS of (10) has the meaning of quasi-particle energy shift at instant t and the second one gives the rate of modulation of the quasiparticle amplitude. Invoking the standard representation of the δ function, $\lim_{t \to \infty} \sin \nu t / \nu = \pi \delta(\nu)$, we get in the limit $t \gg \eta^{-1}$, where η is the minimum excitation energy of $\rho_i(\nu)$:

$$\frac{\partial C_i(t \gg \eta^{-1})}{\partial t} = -i v_i - \Gamma_i. \tag{11}$$

Here,

$$v_i = - \int_{-\infty}^{\infty} \frac{\rho_i(\nu)}{\nu} d\nu, \tag{12}$$

is the relaxation shift of the level energy E_i, and

$$\Gamma_i = \pi \rho_i(0) \tag{13}$$

is the decay rate for the state $|i\rangle$. Hence, in the long-time steady-state limit, the quasiparticle amplitude (8) takes the Markovian form

$$G_i(t \gg \eta^{-1}) \propto e^{\mp i(E_i \pm v_i)t} e^{-\Gamma_i t}. \tag{14}$$

Two complementary quantities that conveniently illustrate temporal propagation of electrons (holes) promoted into unoccupied (occupied) band states are the survival probability $L_i(t)$ of the quasiparticle initial state $|i\rangle$, and the phase $\phi_i(t)$ of its amplitude at the instant t. They are obtained by taking the absolute square and the imaginary part of the logarithm of the corresponding quasiparticle propagator $G_i(t)$ in the real-time domain, respectively [41]. In the notation $|i\rangle = |\mathbf{K}, n\rangle$, the quasiparticle survival probability is given by

$$L_{\mathbf{K},n}(t) = |G_{\mathbf{K},n}(t)|^2, \tag{15}$$

and the associated phase reads

$$\phi_{\mathbf{K},n}(t) = \mp \text{Im} \ln (i G_{\mathbf{K},n}(t)) = E_{\mathbf{K},n} t \pm \varphi_{\mathbf{K},n}(t). \tag{16}$$

Hence, according to (10) and (16), the partial derivative

$$\frac{\partial \varphi_{\mathbf{K},n}(t)}{\partial t} = - \int_{-\infty}^{\infty} \rho_{\mathbf{K},n}(\nu) \frac{1 - \cos \nu t}{\nu} d\nu = v_{\mathbf{K},n}(t) \tag{17}$$

describes the relaxation of quasiparticle energy in the course of time [cf. Eq. (10)].

In the case of a hole created in the occupied band state $|\mathbf{K}, n\rangle$ whose energy $E_{\mathbf{K},n}$ lies below E_F, the second-order cumulant excitation density is given by

$$\rho_{\mathbf{K},n}^{\text{hole}}(\nu) = \sum_{\mathbf{Q}, n'} V_Q^2 \int_0^{\infty} d\omega' \tilde{S}_{n,n';n',n}(\mathbf{Q}, \omega')$$

$$\times \delta(\nu - (E_{\mathbf{K},n} - E_{\mathbf{K}+\mathbf{Q},n'} + \omega')). \tag{18}$$

Here, the summation runs over the occupied band states $|\mathbf{K} + \mathbf{Q}, n'\rangle$, $V_Q = 2\pi/Q$, and the matrix elements $\tilde{S}_{n,n';n',n}(\mathbf{Q}, \omega')$ of the imaginary part of the response function (4) have been defined by Eq. (16) in Sec. II A of Ref. [38]. The thus defined $\rho_{\mathbf{K},n}^{\text{hole}}(\nu)$ is for fixed initial $E_{\mathbf{K},n}$ bounded from below at $\nu_{\min} = E_{\mathbf{K},n} - E_F < 0$, and nonvanishing on
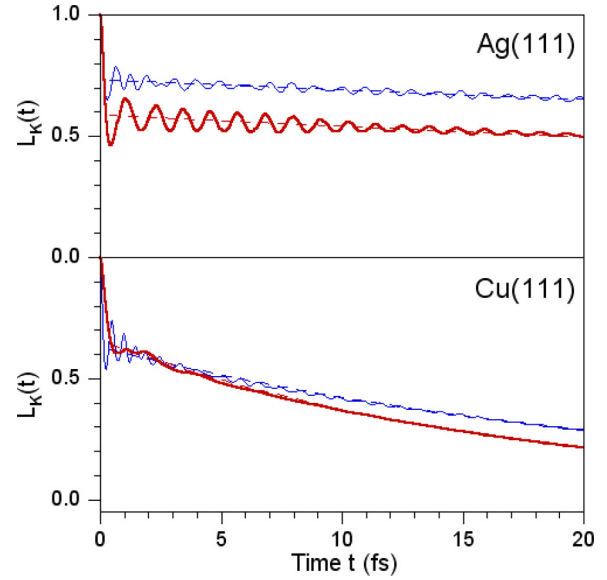

FIG. 4. (Color online) Survival probability $L_{\mathbf{K},\text{SS}}(t)$ for a hole after its promotion into the surface state band on Ag(111) and Cu(111) with the initial state wave vector $K = 0.01$ a.u. corresponding to initial $\epsilon_K^{\text{SS}} = 3$ meV above the respective band bottom. Also shown for comparison are the interpolated Markovian decays of the SS holes (dashed lines) described by expression (20). Thick (thin) solid lines stand for the results obtained with (without) inclusion of the d polarizable medium in the response function evaluation. The values for the decay rates $\Gamma_{\mathbf{K}}$ obtained from the interpolation of Markovian decay in the absence of d-polarizable continuum are in excellent agreement with the ones computed in Table 3 of Ref. [55].

the energy shell $\nu = 0$ where it yields the hole decay rate $\Gamma_{\mathbf{K},n} = \pi \rho_{\mathbf{K},n}^{\text{hole}}(0)$.

Temporal evolutions of the survival probability $L_{\mathbf{K},n}(t)$ [Eq. (15)] and the transient phase derivative $\partial \varphi_{\mathbf{K},n}(t)/\partial t$ [Eq. (17)] calculated using (18) and corresponding to a hole created at the instant $t_0 = 0$ in the SS band on Ag(111) and Cu(111) surfaces are shown in Figs. 4 and 5, respectively. These plots illustrate distinct stages of the dynamics of a hole promoted in a Q2D SS-band with initial $|\mathbf{K}| > 0$. The initial convexity of $L_{\mathbf{K},n}(t)$ is determined by the Zeno behavior [72–74]:

$$L_{\mathbf{K},n}(t \to 0) = e^{-t^2/\tau_Z^2}, \tag{19}$$

where the inverse of Zeno time τ_Z is given by the zeroth moment of the cumulant spectral density [41] $\tau_Z^{-2} = \int_{-\infty}^{\infty} \rho_{\mathbf{K},n}(\nu) d\nu$. The initial quasiparticle evolution taking place within the time-energy uncertainty window is characterized by the off-the-energy-shell transients caused by the virtual high-energy excitations (collective and single pairs) of the respective substrate. This gives rise to a sharp drop of $L_{\mathbf{K},n}(t)$ due to the establishment of the Debye-Waller factor [41] and early oscillations with the approximately femtosecond period. Attenuation of the oscillations and their dephasing arises from the width of surface excitation spectrum and to a much lesser extent from the phase space segment of allowed quasiparticle recoil energies $E_{\mathbf{K}+\mathbf{Q},n'} - E_{\mathbf{K},n}$ [38,39,41]. Past the few femtosecond long interval [i.e., $t > 20$ fs and $t > 5$ in the case of Ag(111) and Cu(111), respectively] the energy
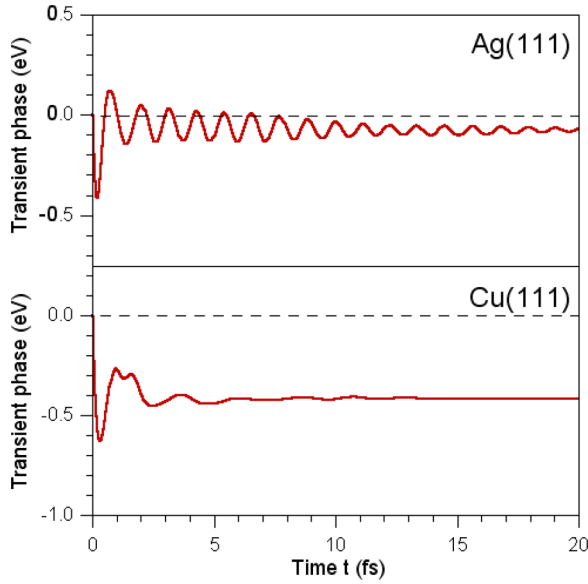
FIG. 5. (Color online) Initial phase transients $\partial \varphi_{\mathbf{K}}(t)/\partial t$, Eq. (17), for a hole promoted into the SS band on Ag(111) and Cu(111) with the initial state wave vector $K = 0.01$ a.u.

conservation sets in and gives rise to phase stabilization and steady-state quasiparticle decay due to the emission of real low-energy e-h excitations in the solid. Here the real or on-the-energy-shell plasmon excitations are not possible because $E_F - E_{\mathbf{K},n} < \hbar\omega_s$. In this intermediate interval, the decay of the initial state described by (15) is Markovian. In accord with (14), it follows exponential law governed by the FGR decay rate corrected (reduced) by the real part of the Debye-Waller exponent [41] $w_{\mathbf{K},\mathrm{SS}}$, viz.

$$L_{\mathbf{K},\mathrm{SS}}^{\mathrm{Mar}}(t) = e^{-2(\Gamma_{\mathbf{K},\mathrm{ss}}t + w_{\mathbf{K},\mathrm{SS}})}. \tag{20}$$

This limit is illustrated in Fig. 4 where its onset can be clearly pinpointed. The already available databases of calculated quasiparticle lifetimes [55,75–78]

$$\tau_{\mathbf{K},n} = \frac{\hbar}{2\Gamma_{\mathbf{K},n}} \tag{21}$$

(here we restored $\hbar$ to facilitate comparisons with literature sources) refer to this intermediate steady-state regime of quasiparticle evolution.

The temporal behavior of the derivatives of quasiparticle phases illustrated in Fig. 5 exhibits early transients in the same interval as the corresponding survival probabilities. The phase stabilization or saturation coincides with and signifies the onset of Markovian decay with lifetime (21) of the quasiparticle (here of a hole) past which the standard description of its amplitude in the form (14) becomes applicable. In the asymptotic limit of very long times, the Markovian decay (20) is succeeded by the so-called "quasiparticle collapse" characterized by a much slower power law decay and the loss of phase identity [41,72].

B. Ultrafast screening of excitonic interactions

To proceed with the description of electron propagation in the intermediate states of OA and MPPE from surface

bands, we note that upon photon-induced electron excitation from an occupied band state, the creation of a hole charge switches on an effective interaction potential acting between the excited electron and the hole. This potential consists of the bare Coulomb or direct potential V_{e-h}^{dir}, and the time-dependent polarization potential $\tilde{V}_{e-h}^{\mathrm{ind}}(t)$ induced by the substrate charge density fluctuations, which arise in response to the sudden creation of the hole charge density. The sum of these two potentials

$$V_{e-h}^{\mathrm{exc}}(t) = V_{e-h}^{\mathrm{dir}} + \tilde{V}_{e-h}^{\mathrm{ind}}(t) \tag{22}$$

gives the total time-dependent two-body screened excitonic interaction that strongly affects the relative motion of the excited quasiparticles on the ultrashort time scale. Since V_{e-h}^{dir} is an instantaneous Coulomb potential, which is readily obtainable (cf. Sec. III C), the time dependence of (22) arises solely from the induced potential $\tilde{V}_{e-h}^{\mathrm{ind}}(t)$ whose properties will be investigated next. We again exploit the symmetry of the problem and work in the mixed $(\mathbf{Q}, z)$ representation with the electron and hole z coordinates denoted by z_e and z_h, respectively (cf. Fig. 4 in Ref. [47]). The induced e-h potential $\tilde{V}_{e-h}^{\mathrm{ind}}(t)$ is obtained from the induced electronic charge density $q^{\mathrm{ind}}(\mathbf{Q}, z_2, t)$, which in the linear response theory is obtained from

$$q^{\mathrm{ind}}(\mathbf{Q}, z_2, t) = \int dz_1 \int dt_1 \chi(\mathbf{Q}, z_2, z_1, t - t_1)$$
$$\times V(\mathbf{Q}, z_1, z_h, t_1), \tag{23}$$

where $V(\mathbf{Q}, z_1, z_h, t_1)$ is the bare Coulomb potential at the point z_1 that is caused by the hole located at z_h, and the limits of integration over t_1 appropriate to the transient response will now be specified. Within the KLA, in which the hole motion is solved first, causality imposes the use of retarded electronic response function $\chi(\mathbf{Q}, z_1, z_2, t - t_1)$ in the evaluation of the induced charge (23) and the ensuing potential. Obeying the temporal boundary conditions for the bare e-h Coulomb interaction switched on with the creation of the pair at $t_1 = 0$, and making use of the FT of spectral representation (4) to the time domain, the calculation of the induced potential reduces to finding the convolution of the switched on bare e-h potential with the response function χ in the interaction interval $0 \leqslant t_1 \leqslant t$ [79]. This gives the reactive (i.e., real or nondissipative) retarded potential acting on the excited electron in the form

$$\tilde{V}_{e-h}^{\mathrm{ind}}(\mathbf{Q}, z_e, z_h, t) = \Theta(t) V_Q^2 \int dz_2 \int dz_1 e^{-Q|z_e - z_2|} e^{-Q|z_1 - z_h|}$$
$$\times \int_0^\infty d\omega' \frac{2}{\omega'} \tilde{\mathcal{S}}(\mathbf{Q}, z_1, z_2, \omega')(1 - \cos\omega' t)$$
$$= \Theta(t) V_Q^2 \int dz_2 \int dz_1 e^{-Q|z_e - z_2|} e^{-Q|z_1 - z_h|}$$
$$\times \int_0^\infty d\omega' \tilde{\mathcal{N}}_{\mathbf{Q}}(z_1, z_2, \omega')(1 - \cos\omega' t), \tag{24}$$

where for the sake of compactness of ensuing notation, we have introduced the spectral density

$$\tilde{\mathcal{N}}_{\mathbf{Q}}(z_1, z_2, \omega') = 2\tilde{\mathcal{S}}(\mathbf{Q}, z_1, z_2, \omega')/\omega'. \tag{25}$$

Eliminating the absolute values in the exponentials by introducing the appropriate lower and upper integration boundaries of z_1 and z_2, we obtain

$$\tilde{V}_{e-h}^{\text{ind}}(\mathbf{Q}, z_e, z_h, t)$$
$$= \Theta(t) V_Q^2 \Bigg[e^{Q(z_e + z_h)} \int_{z_e}^{\infty} dz_2 \int_{z_h}^{\infty} dz_1 e^{-Q(z_2 + z_1)}$$
$$+ e^{-Q(z_e - z_h)} \int_{-\infty}^{z_e} dz_2 \int_{z_h}^{\infty} dz_1 e^{Q(z_2 - z_1)}$$
$$+ e^{Q(z_e - z_h)} \int_{z_e}^{\infty} dz_2 \int_{-\infty}^{z_h} dz_1 e^{-Q(z_2 - z_1)}$$
$$+ e^{-Q(z_e + z_h)} \int_{-\infty}^{z_e} dz_2 \int_{-\infty}^{z_h} dz_1 e^{Q(z_2 + z_1)} \Bigg]$$
$$\times \int_0^{\infty} d\omega' \tilde{\mathcal{N}}_{\mathbf{Q}}(z_1, z_2, \omega')(1 - \cos \omega' t). \quad (26)$$

Here, it should be noted that in the present slab model the effective integration boundaries of z_1 and z_2 extend only few atomic radii outside the slab surfaces beyond which the electron density can be neglected relative to the bulk value.

Several important general features of the dynamics of screening of the suddenly turned on e-h interaction can be readily deduced from expression (26). First, the induced potential (26) starts from zero at $t = 0$ and for $t \to \infty$ saturates at the asymptotic value determined by

$$\tilde{V}_{e-h}^{\text{ind}}(\mathbf{Q}, z_e, z_h, \infty) = V_Q^2 \int dz_2 e^{-Q|z_e - z_2|} \int dz_1 e^{-Q|z_h - z_1|}$$
$$\times \int_0^{\infty} d\omega' \tilde{\mathcal{N}}_{\mathbf{Q}}(z_1, z_2, \omega'). \quad (27)$$

Second, the Fourier inversion of this expression into the $\boldsymbol{\rho}$ space yields the repulsive electron interaction with the stationary electronic polarization cloud induced by the hole. Third, any prominent peak of non-negligible weight in the spectral density $\tilde{\mathcal{N}}_{\mathbf{Q}}(z_1, z_2, \omega')$, and in particular of collective excitations like the various forms of plasmons, gives rise to attenuated oscillations of (26) around the saturation value attained for $t \to \infty$, irrespective of the detailed structure of $\tilde{\mathcal{N}}_{\mathbf{Q}}(z_1, z_2, \omega')$.

Next, we explore the special case of electronic polarization induced interaction $\tilde{V}_{e-h}^{\text{ind}}(\mathbf{Q}, z_e, z_h, t)$ in which z_e and z_h lie in the exterior of the metal, i.e., outside the RHS slab surface where the unperturbed electronic charge density is negligible. In this geometry, only the last term in the square bracket on the RHS of (26) survives due to the effective integration boundaries which straddle the slab. This can be written in a compact form,

$$\tilde{V}_{e-h}^{\text{ind}}(\mathbf{Q}, z_e > 0, z_h > 0, t)$$
$$= V_Q^2 e^{-Q(z_e + z_h)} \int_{\text{slab}} dz_2 e^{Q z_2} \int_{\text{slab}} dz_1 e^{Q z_1}$$
$$\times \int_0^{\infty} d\omega' \tilde{\mathcal{N}}_{\mathbf{Q}}(z_1, z_2, \omega')(1 - \cos \omega' t), \quad (28)$$

which, as shown in the following, will yield the semiclassical analog of the image potential. Noting that $V_Q = 2\pi/Q$, it now turns out convenient to define in the external space $z_e > 0$ and

$z_h > 0$ the surface response function [5] in the form

$$R_{\mathbf{Q}}(\omega) = \frac{2\pi}{Q} \int_{\text{slab}} dz_2 e^{Q z_2} \int_{\text{slab}} dz_1 e^{Q z_1} \chi(\mathbf{Q}, z_1, z_2, \omega'), \quad (29)$$

which coincides with the response function [65] $g(\mathbf{Q}, \omega)$ in (7) and has a Lehmann representation analogous to (4):

$$R_{\mathbf{Q}}(\omega) = \int_0^{\infty} d\omega' S_{\mathbf{Q}}(\omega') \left(\frac{1}{\omega - \omega' + i\delta} - \frac{1}{\omega + \omega' + i\delta} \right). \quad (30)$$

Here, $S_{\mathbf{Q}}(\omega')$ is obtained by using (4) and (25):

$$S_{\mathbf{Q}}(\omega') = \frac{2\pi}{Q} \int_{\text{slab}} dz_1 e^{Q z_1} \int_{\text{slab}} dz_2 e^{Q z_2} \tilde{\mathcal{S}}(\mathbf{Q}, z_1, z_2, \omega')$$
$$= \frac{\omega'}{2} \frac{2\pi}{Q} \int_{\text{slab}} dz_2 e^{Q z_2} \int_{\text{slab}} dz_1 e^{Q z_1} \tilde{\mathcal{N}}_{\mathbf{Q}}(z_1, z_2, \omega')$$
$$= \frac{\omega'}{2} N_{\mathbf{Q}}(\omega'), \quad (31)$$

where in analogy with (25) and for later convenience we have introduced the spectral density of surface projected electronic excitations

$$N_{\mathbf{Q}}(\omega') = \frac{2\pi}{Q} \int_{\text{slab}} dz_2 e^{Q z_2} \int_{\text{slab}} dz_1 e^{Q z_1} \tilde{\mathcal{N}}_{\mathbf{Q}}(z_1, z_2, \omega'). \quad (32)$$

Now, combining (28) and (32), we finally obtain for the electron and hole located outside the slab:

$$\tilde{V}_{e-h}^{\text{ind}}(\mathbf{Q}, z_e, z_h, t) = V_Q e^{-Q(z_e + z_h)}$$
$$\times \int_0^{\infty} d\omega' N_{\mathbf{Q}}(\omega')(1 - \cos \omega' t). \quad (33)$$

Using this expression, we can define the *transient factor*

$$\mathcal{T}(t) = \lim_{\mathbf{Q} \to 0} \int_0^{\infty} d\omega' N_{\mathbf{Q}}(\omega')(1 - \cos \omega' t) \Bigg/ \int_0^{\infty} d\omega' N_{\mathbf{Q}}(\omega'), \quad (34)$$

which describes the dynamics of saturation of an ultrafast screening process by way of the formation of the dominant, long-wavelength component of the stationary screening charge and the induced potential arising thereof. Its temporal variation calculated using the electronic excitation spectra (31) for Cu and Ag surfaces derived in Sec. II is illustrated in Fig. 6. Note here a much faster saturation of the transient factor $\mathcal{T}(t)$, and hence of the corresponding screening charge and induced potential, on the Cu(111) surface relative to the Ag(111) surface. This is due to the different structures of $N_{\mathbf{Q}}(\omega') = 2S_{\mathbf{Q}}(\omega')/\omega'$, which in the case of Cu is dominated by a broad spectral continuum instead of a sharp peak at the reduced surface plasmon frequency [cf. Fig. 3(b)]. It should also be noted that the saturation of transient factors obtained in the present work is somewhat slower than of those presented in Fig. 5 of Ref. [47] and calculated using the semiempirical $N_{\mathbf{Q}}(\omega')$. This is so because the semiempirical ones include also the contributions from higher energy interband transitions which cause additional dephasing and hence faster attenuation of coherent oscillations of $\mathcal{T}(t)$.

The zero and long-time limits of the transient factors shown in Fig. 6 are equal (i.e., 0 and 1, respectively) because they reflect the causality and saturation of screening of external charges outside metal surfaces, respectively. The surface
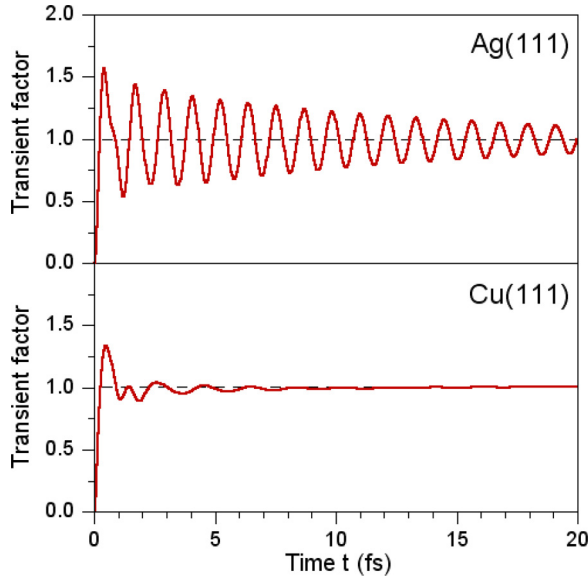
FIG. 6. (Color online) (Top) Transient factor $\mathcal{T}(t)$ defined in Eq. (34) and determining the evolution of polarization induced component of e-h potential acting on the electron upon its promotion in front of Ag(111) surface. The transient oscillatory behavior is caused by an excitation of a virtual surface plasmon which is a well defined excitation in this system (cf. Fig. 2(b) above and Fig. 1 of Ref. [80]). (Bottom) Same for Cu(111) surface. Here the oscillation dephases and saturates much faster because it is governed by a wide spectrum of incoherent electronic excitations (cf. Fig. 3(b) above and Fig. 1 of Ref. [81]).

excitation spectra (31) and (32), which obey the perfect screening sum rule [5]

$$\lim_{\mathbf{Q} \to \mathbf{0}} \int_0^\infty \frac{2}{\omega'} S_{\mathbf{Q}}(\omega') d\omega' = \lim_{\mathbf{Q} \to \mathbf{0}} \int_0^\infty N_{\mathbf{Q}}(\omega') d\omega' = 1 \quad (35)$$

automatically yield the unitarity of the long-time limit of the numerator in (34). Since the property (35) has been demonstrated numerically for a number of real metal surfaces by using the semiempirical $N_{\mathbf{Q}}(\omega')$ reconstructed from optical and transport data (see Sec. III and Table I in Ref. [82]), as well as in the present slab calculations, the unitarity of transient factors in Fig. 6 should represent a general feature.

Due to the isotropy of the slab pseudopotential in the planes parallel to the surface, the dependence of the electronic response and induced potential on the momentum $\mathbf{Q}$ is only through its magnitude $Q = |\mathbf{Q}|$, i.e., we have $\tilde{N}_{\mathbf{Q}}(z_1, z_2, \omega') = \tilde{N}_Q(z_1, z_2, \omega')$ and hence $\tilde{V}_{e-h}^{\text{ind}}(\mathbf{Q}, z_e, z_h, t) = \tilde{V}_{e-h}^{\text{ind}}(Q, z_e, z_h, t)$. This property will be also exploited in all the ensuing calculations. Then, the expression for induced e-h potential in the direct space is obtained by taking the 2D FT of (24), which yields

$$\tilde{V}_{e-h}^{\text{ind}}(\bar{\boldsymbol{\rho}}, z_e, z_h, t) = \int_0^\infty dQ \frac{Q}{2\pi} \int_0^{2\pi} \frac{d\varphi}{2\pi} e^{iQ\bar{\rho}\cos\varphi} \tilde{V}_{e-h}^{\text{ind}}(Q, z_e, z_h, t)$$

$$= \int_0^\infty dQ \frac{Q}{2\pi} J_0(Q\bar{\rho}) \tilde{V}_{e-h}^{\text{ind}}(Q, z_e, z_h, t). \quad (36)$$

Here, $\bar{\boldsymbol{\rho}} = \boldsymbol{\rho}_e - \boldsymbol{\rho}_h = \bar{\boldsymbol{\rho}}_{e-h}$, $\bar{\rho} = |\bar{\boldsymbol{\rho}}|$ and the appearance of Bessel function $J_0(Q\bar{\rho})$ in the integrand on the RHS of (36)

follows from the isotropy of $\tilde{V}_{e-h}^{\text{ind}}(Q, z_e, z_h, t)$, which allows straightforward integration over the polar angle φ.

Fulfilment of the sum rule (35) gives rise to universal forms of the fully relaxed induced potentials acting between the probe charges located outside the surface. This is readily demonstrated by inspecting the long-time limit of expression (33) obtained for $z_e > 0$, $z_h > 0$. The saturated polarization or image induced interaction between the electron and hole charges takes in this case a simple form:

$$\tilde{V}_{e-h}^{\text{ind}}(\bar{\boldsymbol{\rho}}, z_e, z_h, \infty) = \int_0^\infty dQ \frac{Q}{2\pi} V_Q J_0(Q\bar{\rho}) e^{-Q(z_e + z_h)}$$

$$\times \int_0^\infty d\omega' N_Q(\omega'). \quad (37)$$

To estimate the asymptotic form of (37) for the electron and hole point charges located at $(\boldsymbol{\rho}_e, z_e)$ and $(\boldsymbol{\rho}_h, z_h)$ far outside the surface one can use either the perfect screening sum rule (35) verified for real metals [82], or in the case of free electron metal surfaces the model expression [5] $\lim_{Q \to 0} = N_Q(\omega') = \delta(\omega' - \omega_s) + \mathcal{O}(Q)$. Thereby one finds the following leading contribution to the saturated induced polarization potential:

$$\tilde{V}_{e-h}^{\text{ind}}(\bar{\boldsymbol{\rho}}_{e-h}, z_e > 0, z_h > 0, t \to \infty) = \frac{e^2}{\sqrt{\bar{\rho}_{e-h}^2 + (z_e + z_h)^2}}. \quad (38)$$

Expression (38) is the classical result for the polarization induced interaction between two point charges of opposite sign placed in front of an ideal conducting surface whose direct Coulomb interaction is given by (note change of signs)

$$V_{e-h}^{\text{dir}}(\bar{\boldsymbol{\rho}}_{e-h}, z_e > 0, z_h > 0) = -\frac{e^2}{\sqrt{\bar{\rho}_{e-h}^2 + (z_e - z_h)^2}}. \quad (39)$$

Due to the permutation symmetry of z_e and z_h in (37), and consequently in (38), the latter expression can be visualized as the electron interaction with the hole image, or vice versa, the hole interaction with the image of the electron, but should be counted only once in pairwise summations of polarization interactions. The expansion of the sum of (38) and (39) in $1/z_e$ gives the classical limit of residual e-h interaction after completion of screening.

In the general case of a unit positive point charge located at arbitrary position relative to the surface, all four terms in the square bracket on the RHS of (26) must be taken into account in the determination of induced potential. As demonstrated in the Appendix, this enables a generalization of expressions (29) and (37).

To assist the interpretation of temporal features of $\tilde{V}_{e-h}^{\text{ind}}(\bar{\boldsymbol{\rho}} = 0, z_e, z_h, t)$, and thereby of the saturation of screening as z_h moves from the exterior to the interior of the slab we have first computed the corresponding potentials in the bare sp model that leads to the d-unrenormalized surface plasmon dominated response and loss functions shown in Figs. 2(a) and 3(a) for Ag(111) and Cu(111) surfaces, respectively. The thus obtained potentials $\tilde{V}_{e-h}^{\text{ind}}(\bar{\boldsymbol{\rho}} = 0, z_e, z_h, t)$ as a function of z_e and t, with the coordinate z_h of the perturbation source placed at three representative points to illustrate the general case (26) are shown in Figs. 7 and 8. Spacewise this means (a) sufficiently outside the slab where the electron density
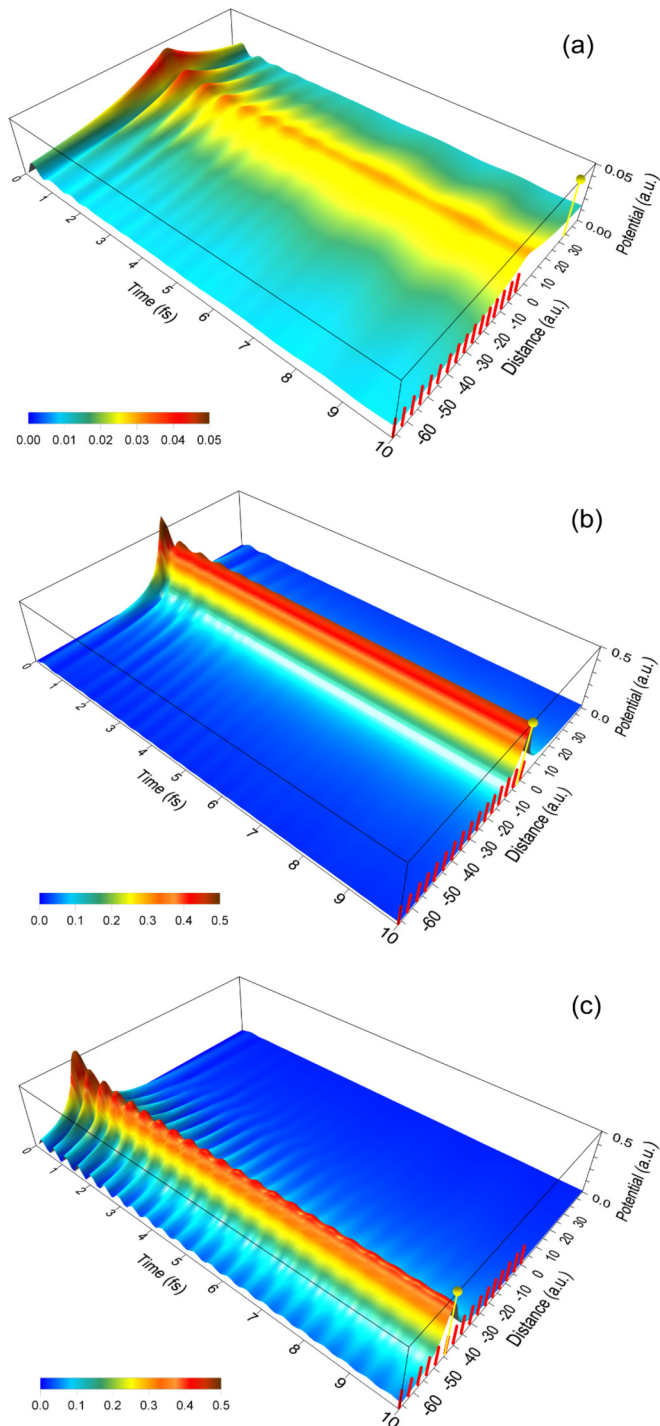
FIG. 7. (Color online) 3D plot of the polarization-induced e-h interaction potential $\tilde{V}_{e-h}^{\text{ind}}(\bar{\rho} = 0, z_e, z_h, t)$ for a Ag(111) surface calculated from Eq. (36) of the main text using the sp model, i.e., without the d renormalization of surface response described at the end of Sec. II. The potential (in atomic units) is shown as a function of z_e and t, for the coordinate z_h (yellow dot) fixed at (a) 7.5, (b) $-\frac{1}{2}$, and (c) -10 interlayer spacings relative to the first crystal plane of the slab located at $z = 0$. Short red vertical lines denote the positions of (111) crystal planes across half of the slab width.
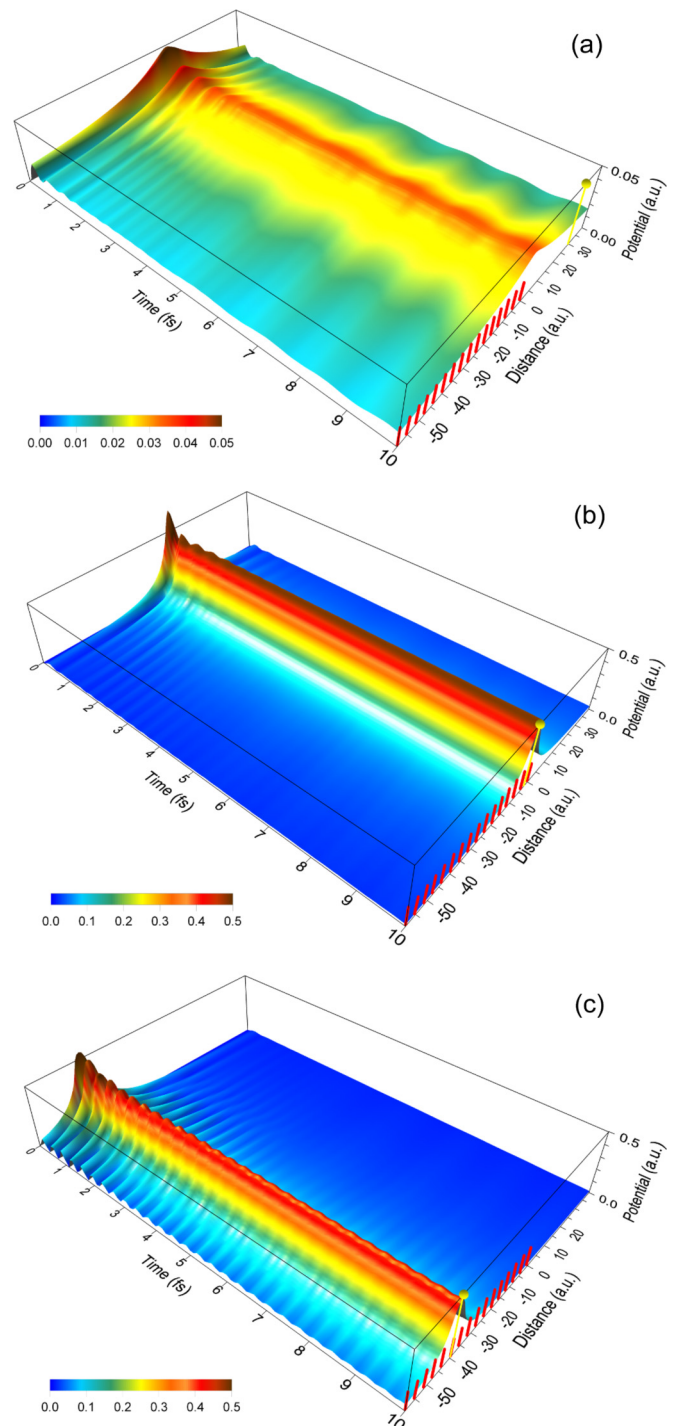

FIG. 8. (Color online) Same as in Fig. 7 but for the Cu(111) surface. Note that in both Figs. 7 and 8 the frequency of oscillation of the potential $\tilde{V}_{e-h}^{\text{ind}}(\bar{\rho} = 0, z_e, z_h, t)$ is lower outside the slab.

is already negligible relative to the bulk, (b) in the surface region where the electron density undergoes strong variation, and (c) sufficiently inside the slab where the bulk properties

dominate. These figures clearly demonstrate that in the simple sp model for the electronic response of the slabs the oscillatory behavior and attenuation of the induced polarization potential $\tilde{V}_{e-h}^{\text{ind}}(\bar{\rho} = 0, z_e, z_h, t)$ for z_h outside the slab surface [panels (a)] are determined by the emission of virtual surface plasmons and incoherent single-particle excitations, respectively. By contrast, for z_h deep inside the slab [panels (c)], the oscillatory behavior is driven by the higher bulk plasmon frequency. For

z_h in the surface region [panels (b)], the situation is more complex in that the screening of source perturbation is now affected by the coupling to both surface and bulk plasmons and to single-particle excitations. The splitting of surface plasmon modes due to the finite slab thickness introduces additional interferences and faster dephasing in the initial oscillatory behavior of dynamical screening of the source.

The above described clear-cut temporal behavior of the induced potential $\tilde{V}_{e-h}^{\text{ind}}(\bar{\rho}=0,z_e,z_h,t)$ obtained from the sp model is lost upon the d renormalization in the spd model. On the Cu(111) surface, d renormalization eliminates the discernible identity of surface plasmons whereas on Ag(111) surface it brings the surface and bulk plasmon frequencies so close to each other that the resolution of their respective effects becomes very difficult. This is shown in Figs. 9 and 10, which show the results of spd-model calculation for the variation of $\tilde{V}_{e-h}^{\text{ind}}(\bar{\rho}=0,z_e,z_h,t)$ as a function of z_e and t for Ag(111) and Cu(111) surfaces, respectively, for the same three values of coordinates of the perturbation source z_h as in Figs. 7 and 8. All four figures 7–10 demonstrate that the induced charge density calculated in either model is in the cases (a) pinned to the surface region and not to the perturbation source, in the cases (b), pinned to the surface where also the source is located, and in the cases (c), pinned to the source as is typical of bulk screening. Thereby our results emphasize the difference in the spatial distribution of the induced screening charge relative to the perturbation source in the bulk and at the surface of a metal. It should also be observed that the temporal dependencies of induced potentials shown in panels (a) and (b) of Figs. 9 and 10 bear general resemblance to the corresponding transient factors in Fig. 6 in that the oscillation patterns of the respective quantities are very similar. However, the induced potentials shown in Figs. 9(b) and 10(b) saturate faster than the analogous transient factors. This is so because in the calculation of (34) for $z_h > 0$ and $z_e > 0$ only a narrow range of $Q \sim 0$ components gives the dominant contribution which saturates due to dephasing caused by the width of spectral constituents of $N_{Q\to0}(\omega')$. By contrast, for z_h at the surface, a larger number of $Q > 0$ components of the electronic response contribute to dephasing of the integrand in (36) which, in turn, gives rise to faster saturation of $\tilde{V}_{e-h}^{\text{ind}}(\bar{\rho}=0,z_e,z_h>0,t)$. This makes the readily obtainable transient factor useful in the estimates of the evolution of screening that is induced by the exterior perturbation sources [Figs. 9(a) and 10(a)].

C. Transient excitons as primary emergent states

An important implication of the results of Sec. III B is that at a metal surface the initial dynamics of a coherently excited e-h pair is strongly affected by the total excitonic potential $V_{e-h}^{\text{exc}}(t)$ defined in (22). At the instant of primary excitation $t = 0^+$, this potential is equal to the bare Coulomb potential V_{e-h}^{dir} whose screening by the build up of $V_{e-h}^{\text{ind}}(t)$ can be estimated from the corresponding transient factor (34). Hence a prerequisite for descriptions of the early propagation of optically excited e-h pairs at surfaces is the assessment of the dynamics of quasiparticles subjected to the excitonic interaction V_{e-h}^{dir}.

The treatment of excitonic interactions in optical excitations of solids is a long standing problem [83], which owing to its many-body complexity [42,50] has been studied within many
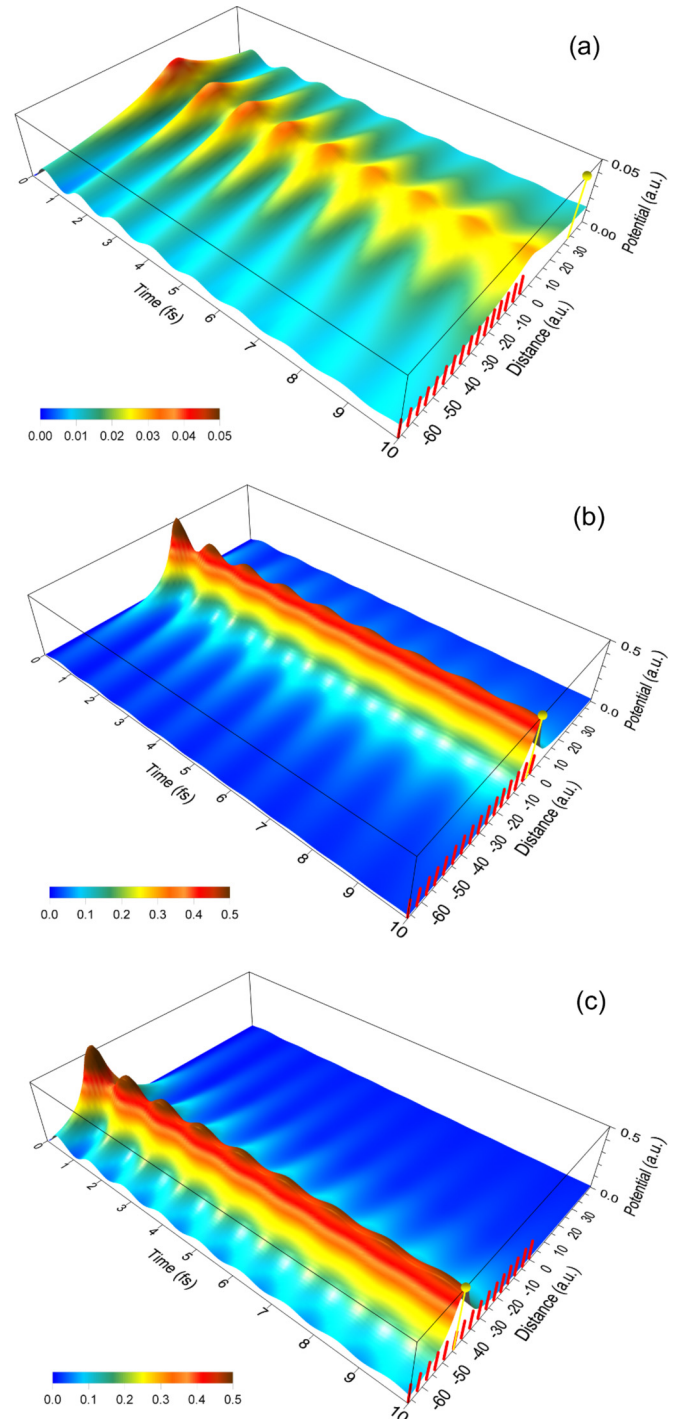

FIG. 9. (Color online) 3D plot of $\tilde{V}_{e-h}^{\text{ind}}(\bar{\rho}=0,z_e,z_h,t)$ for Ag(111) surface calculated from Eq. (36) of the main text using the spd-model, i.e., by including the d renormalization of the surface response described at the end of Sec. II. All other symbols have the same meaning as in Fig. 7.

complementary theoretical approaches [45,46,84–112]. At metal surfaces, the experimentally detectable manifestations of ultrafast dynamics of excitonic interactions between the photoexcited electrons and holes are expected on the time scale of saturation of the screening charge whose duration in a particular system can be estimated from the corresponding transient factor (34).
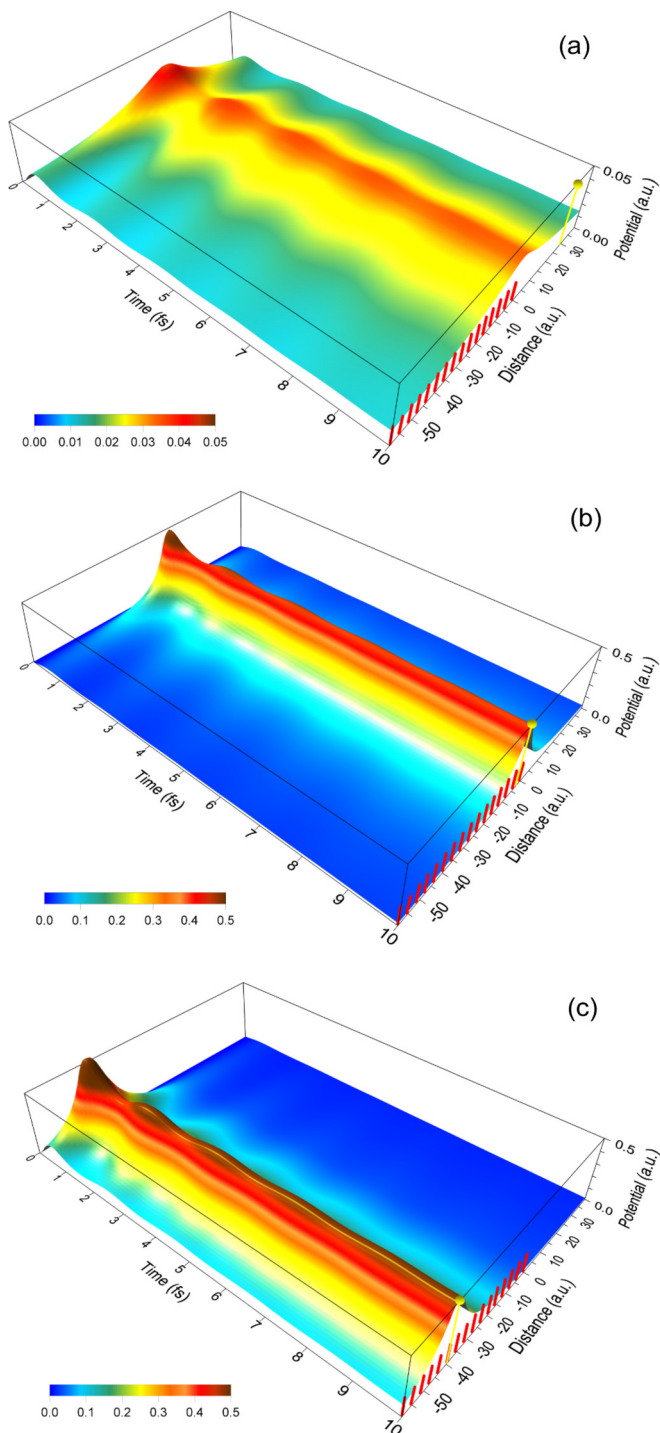
FIG. 10. (Color online) Same as in Fig. 9 but for the Cu(111) surface.

The specificity of the present excitonic problem is the process of optically induced electronic excitations from the occupied states in SS bands on Cu(111) and Ag(111) surfaces [47] as this requires a model description that sufficiently accurately reproduces image charge aspects of the initial state electronic structure. Hence, to assess the energetics of electronic excitations from the SS bands, we shall adopt the same self-consistent pseudopotential model [27] used in Sec. II in the slab calculations of the electronic response of

these surfaces. The pertinent pseudopotential is constructed so as to reproduce the SS band within the surface projected sp-band gap, which is prerequisite for the calculation of energy spectrum of the optically excited electrons and holes bound in the primary excitonic states by the initial unscreened electron-SS hole Coulomb potential [47,69].

Relative motion of electrons and holes created in optically induced interband transitions is generally governed by the many-particle excitonic interaction whose irreducible part consists of the dynamically screened e-h Coulomb attraction and its repulsive unscreened exchange counterpart. Coulomb attraction is the dominant component of primary excitonic interactions [88,90,91]. To remain consistent with application of the slab pseudopotential model and the linear response formalism of Sec. II to the studies of excitonic effects induced by holes in SS bands, we neglect in the following the exchange term from the irreducible electron-hole interaction. This is consistent with the KLA for the hole motion used below and leads to the effective mass approximation (EMA) form of the Schrödinger equation for excitons [85,86,88,93]. In this formulation, the effects of crystal potential on the motion of excited electrons and holes with energies close to the local band extrema are modeled through the effective masses in the kinetic energy terms, and the dynamical electron-SS hole interaction is given by the sum of the bare Coulomb attraction and the induced potential (36).

At the instant $t = 0$ of electron-hole pair excitation, the induced potential is zero and hence the energy spectrum of primary states into which the electrons can be excited consists of the excitonic levels derived from the two-particle Schrödinger equation containing the unscreened effective Coulomb potential of the photoexcited hole charge density [45,47]. In the present problem of electron excitation from the SS-bands on Ag(111) and Cu(111) surfaces, this leads to the following form of the total exciton wave function consistent with the KLA and EMA [47,69,85,86]:

$$\Psi^{\text{EMA}} = \sum_{i,j} F_{i,j} \psi_{B_i} \psi_{SS_j}. \qquad (40)$$

Here, i runs over the quantum numbers at unoccupied band minima B_i, which can support excitons, the wave functions of preexistent electron states at B_i are denoted by ψ_{B_i} and of the jth SS-hole state by ψ_{SS_j}. The 2D spatial Fourier transforms of $F_{i,j}$ describe relative e-h motion in lateral coordinates $\bar{\boldsymbol{\rho}} = \boldsymbol{\rho}_e - \boldsymbol{\rho}_h$ under the action of the effective potential $V_{e-h}^{\text{eff}}(\bar{\boldsymbol{\rho}}, z_e)$ exerted by the SS hole [47]. In this case, the relevant energy zero for excitonic bound state spectrum is the energy ε_{B_i} of the electron state at B_i. At the inner side of Cu(111) and Ag(111) surfaces, this occurs at the bottom U_{sp} of the unoccupied part the sp band above the surface projected band gap (see Table I), whereas at the outer side of the surface it occurs at the vacuum level energy E_V. Since in the present slab model the localization of SS hole is largely within the inner part of the surface pseudopotential (see Fig. 1 in Ref. [38] and Fig. 11 above), the strongest hole interaction is expected with the electrons in the states deriving from the gap edge U_{sp} and leads to the exciton energy spectrum with $\varepsilon_B = U_{sp}$.

The magnitudes of discrete excitonic bound state energies below ε_B are reduced relative to the hydrogenic ones for the same values of the effective e-h mass owing to the finite extension of SS-hole charge density and its anisotropy
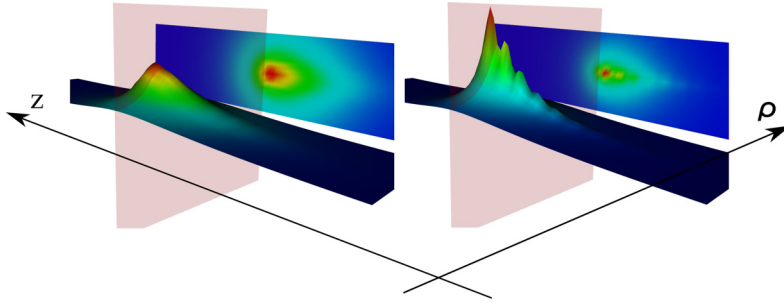
FIG. 11. (Color online) Side and top views of the three-dimensional contour plots illustrating the anisotropy of the modulus of unscreened Coulomb potential exerted by the SS hole on the excited electron in the case of Ag(111) and Cu(111) surfaces (left and right panels, respectively). Positive direction of the z axis is towards the exterior of the metal and the coordinate $|\bar{\boldsymbol{\rho}}|$ is perpendicular to it and to the common vertical axis. Light shaded sheets denote the first surface plane of the crystal occupying the region of the viewer.

in the direction perpendicular to the surface (see Fig. 11). The higher lying bound states constitute a Rydberg- or Kepler-like quasicontinuum of states due to the dominance of monopole term in the primary unscreened e-h Coulomb potential. Subsequent evolution of the induced e-h potential (36) leads to complete screening of the monopole term in the bare e-h Coulomb potential so as that in the long-time limit only a dipolar contribution perpendicular to the surface may survive in the total fully screened e-h interaction. The strength of dipolar interaction is determined by the position of the centroid of hole image charge relative to that of the hole charge and is small in the case of SS holes on Ag(111) and Cu(111) surfaces. If such residual dipolar component of the total e-h potential acted alone, it would produce a much narrower and less dense spectrum than that of primary excitonic levels. In reality, however, this spectrum is overrun by the spectrum of emergent electron image potential $\tilde{V}_{e-e}^{\text{ind}}(z_e,t)$, which, when fully developed, is dominantly monopolar and hence only weakly perturbed by the residual e-h potential (see Sec. III D).

The present computations of the energetics of primary excitonic states on Ag(111) and Cu(111) surfaces proceed by invoking the KLA to solve first the hole dynamics in preexistent SS-band states as described in Sec. III A. In the next step, EMA is employed to describe excited electron dynamics in the states above U_{sp} (cf. Sec. 2.3. in Ref. [47]). This leads to the following Schrödinger equation for the relative e-h motion in the component of excitonic wave function (40) associated with the sp-band gap:

$$\left[-\frac{\hbar^2 \nabla_{\bar{\boldsymbol{\rho}}}^2}{2\mathcal{M}} - \frac{\hbar^2}{2m_e} \frac{\partial^2}{\partial z_e^2} + V_{e-h}^{\text{dir}}(\bar{\boldsymbol{\rho}},z_e) \right] F(\bar{\boldsymbol{\rho}},z_e) = \epsilon F(\bar{\boldsymbol{\rho}},z_e).$$

(41)

This equation comprises the effective e-h mass $\mathcal{M} = m_e^* m_{\text{SS}}^* / (m_e^* + m_{\text{SS}}^*)$ and the effective e-h Coulomb potential induced by the positive SS-hole charge density. The values of electron effective masses m_e^* and m_{SS}^* in lateral directions are taken the same as in the calculation of response function (2), see Table I. For Cu(111) surface, this gives $\mathcal{M}_{\text{Cu}} = 0.33$, and for Ag(111) surface, $\mathcal{M}_{\text{Ag}} = 0.28$. The effective direct electron-SS hole Coulomb potential is obtained from

$$V_{e-h}^{\text{dir}}(\bar{\boldsymbol{\rho}},z_e) = -e^2 \int dz_h \frac{|\psi_{\text{SS}}(z_h)|^2}{\sqrt{\bar{\boldsymbol{\rho}}^2 + (z_e - z_h)^2}},$$

(42)

where $\psi_{\text{SS}}(z_h)$ is the SS-hole wave function defined in Sec. II. Contour plots of the potentials (42) corresponding to Ag(111) and Cu(111) surfaces are shown in Fig. 11. Due to the rotational and reflection symmetry of the potential (42) relative to the coordinate axis and the plane normal to the surface

the eigenfunctions $F_N(\bar{\boldsymbol{\rho}},z_e)$ of (41) exhibit σ, π, $\cdots$ etc. type of symmetry and the corresponding degeneracy. The eigenenergies and eigenfunctions were computed using the grid Hamiltonian method [113] combined with the implicitly restarted Lanczos diagonalization as implemented in the ARPACK code [114,115]. A direct product grid with dimension $75 \times 75 \times 95$ in x, y, and z directions and in the range between -39.2 and 39.2 Å was used. The thus computed values of several lowest bound state energies ϵ_N measured relative to pertinent ε_B are listed in Table II and depicted in Fig. 12. These bound state energies are in good semiquantitative agreement with the results obtained for unscreened excitons in bulk Cu with the hole charge density of similar extension [45].

The total exciton energy in the present effective mass-two band model is expressed as

$$E_{\mathbf{P},N} = \varepsilon_B + \frac{\mathbf{P}^2}{2(m_e + m_{\text{SS}})} + \epsilon_N - E_{\text{SS}},$$

(43)

where $\mathbf{P} = \mathbf{P_e} + \mathbf{P_h}$ is the total 2D exciton momentum parallel to the surface [116]. In optical excitations $\mathbf{P}$ equals the absorbed photon momentum and hence for all practical purposes can be set equal to zero. In this case, the excitonic energy levels cannot themselves introduce dispersion in the spectra of multiphoton induced excitations proceeding via excitonic intermediate states [48].

Making use of the solutions of Eq. (41), we can define a measure of the lateral extension or effective radius of the primary surface exciton in the Nth excited state by

$$\bar{\rho}_N = \frac{\int \bar{\rho} d^2\bar{\boldsymbol{\rho}} \int dz_e |F_N(\bar{\boldsymbol{\rho}},z_e)|^2}{\int d^2\bar{\boldsymbol{\rho}} \int dz_e |F_N(\bar{\boldsymbol{\rho}},z_e)|^2}.$$

(44)

The values of few lowest $\bar{\rho}_N$ on Cu(111) and Ag(111) are also listed in Table II. A completely analogous calculation of ϵ_N and $\bar{\rho}_N$ can be performed in the case of primary excitonic states associated with the vacuum level, i.e., for $\varepsilon_B = E_V$. An alternative but complementary measure of spatial extension of bulk transient excitons is presented in Fig. 6 of Ref. [112].

The time interval during which the excitonic energy levels shown in Table II develop into those corresponding to the fully screened or residual e-h potential can be assessed from the transient factors (34) of respective surfaces. However, as pointed out above and further elaborated in the next section, a simultaneous process of the formation of electron image potential proceeds at the same pace. Hence, within the interval of variation of the transient factor, the excited electron dynamics is jointly governed by the waning e-h potential (22) and the rising electron image potential till the takeover by the latter past the time of final saturation of screening. The

TABLE II. First few primary or unscreened excitonic bound state energies ϵ_N and effective radii $\bar{\rho}_N$ at Ag(111) and Cu(111) surfaces calculated using the KLA and effective mass approximation in the calculations of the SS-hole wave function and energy. Exciton energies are measured from the local minimum ε_B of the sp band above the surface projected band gap. The π-symmetry states are doubly degenerate. For $N \to \infty$, the corresponding excitonic state energies ϵ_N make a Rydberg-like or Kepler-like quasicontinuum below ε_B.

N(symmetry)	Ag(111)	Cu(111)
1(σ)	$\epsilon_1 = -2.6769$ eV, $\bar{\rho}_1 = 5.8787$ a.u.	$\epsilon_1 = -3.1990$ eV, $\bar{\rho}_1 = 4.8436$ a.u.
2(σ)	$\epsilon_2 = -1.7301$ eV, $\bar{\rho}_2 = 7.2745$ a.u.	$\epsilon_2 = -1.9529$ eV, $\bar{\rho}_2 = 6.2513$ a.u.
3(σ)	$\epsilon_3 = -1.1777$ eV, $\bar{\rho}_3 = 9.9740$ a.u.	$\epsilon_3 = -1.2932$ eV, $\bar{\rho}_3 = 9.2151$ a.u.
4(π)	$\epsilon_4 = -0.9886$ eV, $\bar{\rho}_4 = 16.1285$ a.u.	$\epsilon_4 = -1.1260$ eV, $\bar{\rho}_4 = 13.9093$ a.u.
5(σ)	$\epsilon_5 = -0.8777$ eV, $\bar{\rho}_5 = 13.0874$ a.u.	$\epsilon_5 = -0.9641$ eV, $\bar{\rho}_5 = 12.1562$ a.u.
6(σ)	$\epsilon_6 = -0.6759$ eV, $\bar{\rho}_6 = 24.4446$ a.u.	$\epsilon_6 = -0.7753$ eV, $\bar{\rho}_6 = 21.8582$ a.u.
7(π)	$\epsilon_7 = -0.6608$ eV, $\bar{\rho}_7 = 20.4261$ a.u.	$\epsilon_7 = -0.7263$ eV, $\bar{\rho}_7 = 17.5144$ a.u.

emergent quasiparticle spectrum undergoes a transformation from the primary spectrum of excitonic levels reflecting initial strongly correlated and coherent e-h states, to secondary spectra of largely uncorrelated and decohering IP-electron and SS-hole states [38].

D. Temporal evolution of electron image charge and formation of image potential states

To obtain the potential arising from electron interaction with its own induced polarization charge that for exterior electrons has a classical analog of the image charge, we substitute $z_h = z_e$ and $\bar{\rho} = 0$ in (27) and take into account the minus sign and the factor $\frac{1}{2}$ due to self-interaction [the latter factor is automatically accounted for in expressions (10)–(12)]. For an arbitrary position of z_e, this gives in the real space

$$\tilde{V}_{e-e}^{\text{ind}}(z_e,t) = -\frac{1}{2} \int_0^\infty dQ \frac{Q}{2\pi} V_Q^2 \int dz_2 e^{-Q|z_e-z_2|}$$
$$\times \int dz_1 e^{-Q|z_e-z_1|} \int_0^\infty d\omega' \tilde{\mathcal{N}}_Q(z_1,z_2,\omega')$$
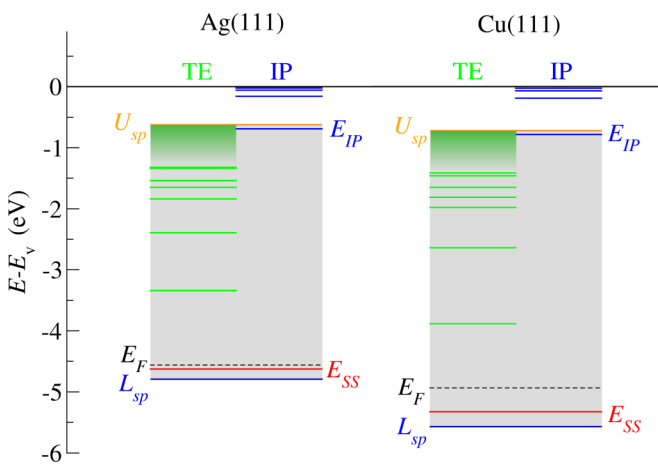$$\times (1 - \cos\omega' t). \tag{45}$$

FIG. 12. (Color online) Energetics of primary excitonic and fully relaxed IP states on Cu(111) and Ag(111) surfaces. Dark green shaded regions in the TE columns symbolize the quasicontinuum of Rydberg-like excitonic states accumulating towards the upper edge U_{sp} of the surface projected bulk sp-band gap [cf. Fig. 1(a)]. Light shaded regions denote extension of the gap on the respective surface.

Note the connection between the temporal dependence of induced self-interaction (45) and of the energy relaxation of quasiparticles injected into the surface bands that are given by the first term on the RHS of expression (10). Spatial variation of the saturated form of the potential (45) across the (111) surface of Cu and Ag slabs is shown in Figs. 13 and 14, respectively. In the exterior, the potentials converge fast to the asymptotic form of the image potential discussed in the remainder of this section.

The formation of standard image potential is retrieved from (45) for z_e outside the spillover of the electronic charge density across the surface plane here placed at $z = 0$. Making use of the definition (31), we have

$$\tilde{V}_{e-e}^{\text{im}}(z_e > 0,t) = -\frac{1}{2} \int_0^\infty dQ \frac{Q}{2\pi} V_Q^2 e^{-2Qz_e} \int_0^\infty d\omega'$$
$$\times \int_{\text{slab}} dz_2 e^{Qz_2} \int_{\text{slab}} dz_1 e^{Qz_1} \tilde{\mathcal{N}}_Q(z_1,z_2,\omega')$$
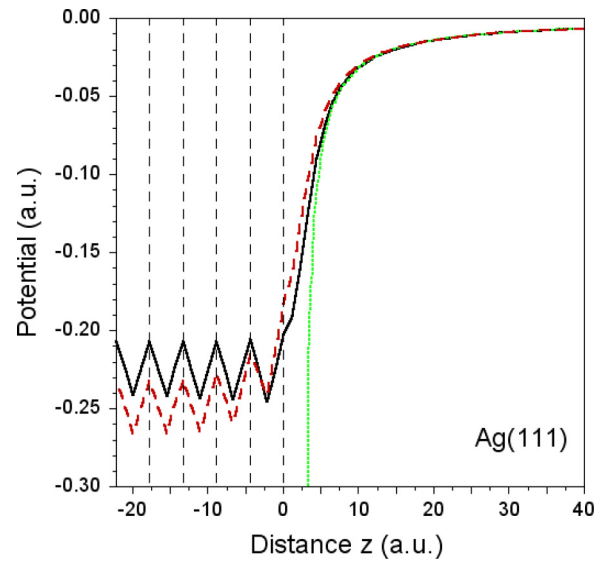
FIG. 13. (Color online) Saturated form of the polarization-induced potential (45) across the Ag(111) surface calculated in the sp (full black line) and spd (dashed red line) models. Outside the surface both potentials converge towards the asymptotic form of image potential (50) (dotted green line). Thin vertical dashed lines denote the positions of (111) crystal planes.
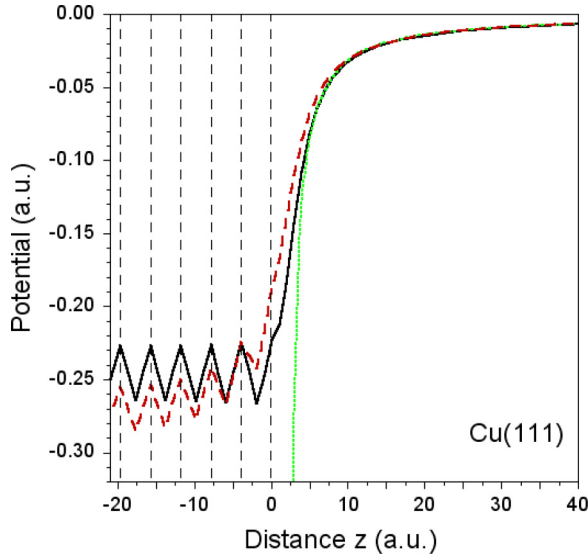
FIG. 14. (Color online) Same as in Fig. 13 but for the Cu(111) surface.

$$\times (1 - \cos \omega' t)$$
$$= -\frac{1}{2} \int_0^\infty dQ e^{-2Qz_e} \int_0^\infty d\omega' N_Q(\omega')$$
$$\times (1 - \cos \omega' t). \qquad (46)$$

Hence, for electrons excited into the region outside the surface, the pace of formation of the two screening potentials, viz. the image potential (46) and the induced e-h polarization potential (33) that screens the bare e-h excitonic potential, is governed by the *same transient factor* (34). This plausible but nontrivial finding is the central result of the present work, which enables us to consider the waning of the excitonic potential and the rise of the image potential as two simultaneous processes in which the former gives way to the latter on the common time scale. The transformation of the corresponding spectra of bound states proceeds in the same interval.

Using (46), we obtain in the limit $t \to \infty$ the saturated image potential

$$\tilde{V}_{e-e}^{\mathrm{im}}(z_e) = -\frac{1}{2} \int_0^\infty dQ e^{-2Qz_e} \int_0^\infty d\omega' N_Q(\omega')$$
$$= \frac{1}{2} \int_0^\infty dQ e^{-2Qz_e} R_Q(0). \qquad (47)$$

The reason for expressing the RHS of (47) in terms of $R_Q(\omega = 0)$ obtainable from (29) is to emphasize the established static limit of saturated surface screening. The advantage of more compact forms (46) and (47) relative to the generating expression (45) is in that they can also be calculated using the semiempirical $N_Q(\omega')$ available for a number of metal surfaces [82]. Hence the quantity

$$q^{\mathrm{im}}(Q,\omega') = N_Q(\omega') \qquad (48)$$

represents the spectral and wave-vector decomposition of the image polarization charge induced in the slab by the external point charge. Thereby $N_Q(\omega')$ provides a complete information

on the electronic polarization in response to the application of external probe charge, inasmuch as does $\tilde{\mathcal{N}}_Q(z_1,z_2,\omega')$ in the case of arbitrary position of the perturbing point charge relative to the surface.

Likewise in (38), the classical result for the asymptotic form of electron image potential is obtained by making use of the sum rule (35) in expression on the RHS of (47), or in the case of free-electron metals by substituting $\lim_{Q \to 0} N_Q(\omega') = \delta(\omega' - \omega_s) + \mathcal{O}(Q)$ therein. Restoring the electron charge e this gives

$$\tilde{V}_{e-e}^{\mathrm{im}}(z_e \to \infty) = -\frac{e^2}{4z_e}. \qquad (49)$$

The leading correction to (49) is obtained by taking into account the dispersion $\omega_s = \omega_Q$ of surface plasmon pole (or the maximum) in $N_Q(\omega')$. This gives the reference distance for the image potential with respect to the centroid z_{im} of the static induced surface screening charge [11]

$$\tilde{V}_{e-e}^{\mathrm{im}}(z_e \gg z_{\mathrm{im}}) = -\frac{e^2}{4(z_e - z_{\mathrm{im}})}. \qquad (50)$$

This form of image potential is in accord with the results of Refs. [6,7,11] as well as with the numerical estimates of the asymptotic form of (47) shown in Figs. 13 and 14. Thereby our results for the self-consistent linear response of sp,d electrons in thick Ag(111) and Cu(111) slabs do not point towards the controversy related to the form of relaxed image potential raised in Ref. [117]. Inclusion of (50) into the exterior asymptotic form of the slab pseudopotential [27] yields the energies of relaxed IP-states shown in Fig. 12.

Within the linear response theory, the total potential acting on the electron past the instant $t = 0$ of its excitation from a state in SS-band is composed of the direct instantaneous Coulomb e-h potential and two polarization induced potentials (36) and (45). The temporal dependence of the sum of these three potentials for exterior z_e and z_h (cf. Fig. 6 in Ref. [47]), which takes place on the time scale of variation of the corresponding transient factor (34), gives rise to evolution of the emergent electron states from the primary excitonic to the fully relaxed image potential states with a much narrower spectrum of the bound states. This global picture also persists in the case of weak residual dipolar e-h interactions discussed in the first paragraph of Sec. III C. The limits of the spectra for $t = 0$ and t exceeding the screening saturation time t_s are shown in Fig. 12.

The electronic eigenstates in the interval between $t = 0$ and $t = t_s$ span the adiabatic basis with rapidly varying geometric and dynamic phases [118,119] that in applications should be computed for each instant of time. This is a formidable task due to which such adiabatic states are very impractical for concrete calculations. The alternative Landau-Zener approach [120,121] in terms of the asymptotic quasistationary diabatic electronic states derived from the time-dependent excitonic and image potentials turns out more convenient. Here, the asymptotic eigenstates correspond to those yielding the spectra of the form depicted in Fig. 12, and the diabatic crossing of the potentials takes place within the saturation interval $(0,t_s)$ of the transient factor. This scenario of electronic propagation

from primary excitonic to relaxed image potential states also allows the treatment of electron propagation in emergent states using the formalism elaborated in Ref. [41] for preexistent states. This approach was employed in Sec. S3 of Ref. [48] for description of the intermediate stages in 3PPE from the SS-band on Ag(111). For a more expanded description see Ref. [122].

IV. SUMMARY AND DISCUSSION

In this work, we have formulated a theoretical framework for the description of ultrafast electron dynamics and screening that should prove useful in the interpretations of time- and energy-resolved spectroscopic studies of surfaces of metals and degenerate semiconductors. A concrete application of the formalism was demonstrated for Ag(111) and Cu(111) surfaces in order to provide conceptual and quantitative support to the interpretation of recent time-resolved multiphoton photoemission measurements [15,48], which indicated the observability of transient excitons on surfaces with sufficiently long screening saturation time [48]. To this end, we have studied several temporal stages of screening of quasiparticles and quasiparticle pairs excited in surface bands in the course of an MPPE experiment. Adopting the surface electronic response formalism developed in Sec. II, we have first studied in Sec. III A the effects of screening on the ultrafast dynamics of holes created by absorption of pump photons in the occupied portions of preexistent surface state bands on Ag(111) and Cu(111). The results have revealed that owing to large differences in the dynamics of electronic response of these two surfaces the hole dynamics in the respective SS bands should also exhibit notable differences which, in turn, should affect the primary steps of ultrafast pump-probe experiments in the two cases. In the next step, we have investigated in Sec. III B the temporal evolution of screening of the Coulomb interaction acting between an electron and a hole photoexcited in the surface region by a pump photon. Likewise in the case of single quasiparticles, we have found that surface screening of bare e-h Coulomb interaction saturates within only few ($\sim$5) femtoseconds on Cu(111) surface, whereas on Ag(111), this process takes much longer ($\sim$15–20 fs). To facilitate visualization of the screening dynamics at dielectric surfaces we have introduced the notion of transient factor which quantitatively estimates the duration of formation and saturation of the screening charge. Sufficiently long saturation time on Ag(111) surface makes possible the observation of binding of photoexcited e-h pairs in transient surface excitons [47,48]. Implications of this result may be extended beyond the studied Ag(111) surface to other systems exhibiting screening saturation times of the order of tens or hundreds of femtoseconds that can occur in low density impurity or photodoped plasmas in semiconductors [16,123]. Following this concept, we have calculated in Sec. III C the energy spectra of coherent unscreened or primary excitonic states which in the course of screening evolve into the energy spectrum of incoherent IP-electron and SS-hole pairs. The latter aspect was elaborated in Sec. III D where we have complemented our studies with the assessment of dynamics of formation of electron image charge and the corresponding potential, which supports the spectrum of emergent IP states on Cu(111) and Ag(111) surfaces. Here

we establish the main result of our work that due to the general temporal properties of screening at surfaces the waning of the excitonic potential and the rise of the image potential proceed on the common time scale governed by the same transient factor.

The scenario in which the spectra of primary excitonic states evolve into the spectra of emergent IP states on the time scale of the substrate specific transient factor underlies the interpretation of interferometric MPPE measurements that have revealed the existence of transient excitons on metal surfaces (cf. Figs. 2, 4, S2 in Ref. [48], and Supplemental Material [122] supported by Refs. [124–131]). From the calculated evolution of the induced potentials one can now contemplate experimental situations and observables where the excitonic response of metals might be observed. In linear spectroscopy with light interacting with metals, below the interband absorption threshold, our theory of the excitonic response predicts that no bound states can exist on time scales defined either by screening or energy time uncertainty, where the relevant energy is detuned from an energy conserving interband transition. The transient polarization will decay by the coherent e-h recombination to produce the coherent replica of the incoming field, i.e., the reflected field, unless it is resonant with an energy conserving emergent state, such as the image potential state.

In a nonlinear experiment, the metallic surface can be investigated during the different time scales of the corresponding transient factor. Any metal with a typical metallic density of electrons will exhibit subfemtosecond screening transients such as shown for Ag(111) and Cu(111) surfaces in Fig. 6, where the screening charge density reaches the asymptotic value over a sequence of overshooting and undershooting cycles. Given the <100 as pulse durations from state-of-the-art lasers, one can anticipate that screening transients of excitonic wave packets, where the system evolves from and oscillates between bound to over screened excitonic states might be observable as an oscillation in photoemission energy spectrum at the frequencies of the transient factor. Such experiments remain a challenge to attosecond spectroscopy. Even in the case where the oscillations of the transient factor are not resolved, it is evident that the screening dynamics can be observed in femtosecond multidimensional multiphoton photoemission spectroscopy, as was recently demonstrated for the Ag(111) surface [48]. There the exciton is revealed through its dispersionless energy-momentum distribution in photoemission spectra at the two-photon resonance from SS to the emergent IP sate. This observation can be rationalized by the oscillation of the transient factor about the saturation value on 10–20 fs time scale, which apparently preserves the electron-hole correlation even though on the average the Coulomb potential is fully screened. The signature of the correlation appears in the momentum space as a nondispersive spectrum rather than in the energy space as a residual binding energy with respect to the reference energy U_{sp}.

The present theoretical framework illuminates that the screening time scale is not just determined by the plasma frequency, as one can read in any solid state physics textbook, but also by the plasma dephasing, which leads to the establishment of steady screening charge. We note that the transient screening dynamics described in the preceding sections are universal in

any condensed matter system, whether or not bound excitons exist. In any solid state system, there will exist a transient regime associated with the retarded material response function. The metallic free electron densities make experimental measurement of the transient screening response challenging, but the transient regime is readily accessible in degenerate impurity and photodoped semiconductors [16]. Thus we believe the theoretical ideas presented in this work are readily testable by the appropriate choice of experimental techniques and materials.

APPENDIX: GENERALIZATION OF EQ. (29)

The long-time or saturation limit of expression (37) can be generalized to the case of arbitrary positions of z_e and z_h. Making use of (27), we may write for the saturated induced potential

$$\tilde{V}_{e-h}^{\text{ind}}(Q,z_e,z_h,t \to \infty) = V_Q e^{-Q(z_e+z_h)}\left[\int dz_2 e^{-Q(|z_e-z_2|-z_e)} \int dz_1 e^{-Q(|z_h-z_1|-z_h)} \int_0^\infty d\omega' \frac{2\pi}{Q}\tilde{\mathcal{N}}_{\mathbf{Q}}(z_1,z_2,\omega')\right]. \quad (A1)$$

In the limit $z_e \gg z_2$ and $z_h \gg z_1$, this expression reduces to expression (37), as it should. Hence the double spatial integral in the square bracket on the RHS of (A1) can be considered as the generalization of the static limit of (30) for arbitrary positions of z_e and z_h. This enables us to define its dynamic counterpart in the following equivalent forms:

$$\tilde{\mathcal{R}}_{\mathbf{Q}}(\omega) = \frac{2\pi}{Q}\int dz_2 e^{-Q(|z_e-z_2|-z_e)}\int dz_1 e^{-Q(|z_h-z_1|-z_h)}\int_0^\infty d\omega' \tilde{\mathcal{S}}_{\mathbf{Q}}(z_1,z_2,\omega')\left(\frac{1}{\omega-\omega'+i\delta}-\frac{1}{\omega+\omega'+i\delta}\right)$$

$$= \frac{2\pi}{Q}\int dz_2 e^{-Q(|z_e-z_2|-z_e)}\int dz_1 e^{-Q(|z_h-z_1|-z_h)}\chi(\mathbf{Q},z_1,z_2,\omega')$$

$$= \frac{2\pi}{Q}\int dz_2 e^{-Q(|z_e-z_2|-z_e)}\int dz_1 e^{-Q(|z_h-z_1|-z_h)}\int_0^\infty d\omega' \tilde{\mathcal{N}}_{\mathbf{Q}}(z_1,z_2,\omega')\frac{\omega'^2}{\omega^2-\omega'^2+i\delta}. \quad (A2)$$

For $z_e = z_h$, this expression is continuous across the surface and hence can be tested against the sum rules [1] likewise its exterior limit $R_{\mathbf{Q}}(\omega)$. The perfect screening sum rule is obtained in the limit $\omega \to 0$, and the f-sum rule as the coefficient of $1/\omega^2$ in the expansion of (A2) in the limit $\omega \to \infty$.

[1] D. Pines and P. Nozières, *The Theory of Quantum Liquids* (Benjamin, New York and Amsterdam, 1966), Vol. I, Ch. 2.3.

[2] G. D. Mahan, *Many Particle Physics* (Plenum Press, New York and London, 1981), Chaps. 6 and 7.

[3] P. Nozières and C. T. De Dominicis, Phys. Rev. **178**, 1097 (1969); and references therein.

[4] J. W. Gadzuk, in *Photoemission and the Electronic Properties of Surfaces*, edited by B. Feuerbacher, B. Fitton and R. F. Willis, (Wiley, Chichester, 1978), Chap. 5.

[5] B. Gumhalter, Prog. Surf. Sci. **15**, 1 (1984); see Secs. 2A and 2B.

[6] D. M. Newns, Phys. Rev. B **1**, 3304 (1970).

[7] D. E. Beck and V. Celli, Phys. Rev. B **2**, 2955 (1970).

[8] J. A. Appelbaum and D. R. Hamann, Phys. Rev. B **6**, 1122 (1972).

[9] N. D. Lang and W. Kohn, Phys. Rev. B **7**, 3541 (1973).

[10] N. D. Lang and A. R. Williams, Phys. Rev. B **16**, 2408 (1977).

[11] A. Liebsch, *Electronic Excitations at Metal Surfaces* (Plenum Press, New York, 1997).

[12] V. M. Silkin, A. K. Kazansky, E. V. Chulkov, and P. M. Echenique, J. Phys.: Condens. Matter **22**, 304013 (2010).

[13] R. D. Muiño, D. Sánchez-Portal, V. M. Silkin, E. V. Chulkov, and P. M. Echenique, Proc. Natl. Acad. Sci. USA **108**, 971 (2011).

[14] H. Petek and S. Ogawa, Prog. Surf. Sci. **56**, 239 (1997).

[15] S. Ogawa, H. Nagano, H. Petek, and A. P. Heberle, Phys. Rev. Lett. **78**, 1339 (1997).

[16] R. Huber, F. Tauser, A. Brodshelm, M. Bichler, G. Abstreiter, and A. Leitenstorfer, Nature (London) **414**, 286 (2001).

[17] J. Güdde, M. Rohleder, T. Meier, S. W. Koch, and U. Höfer, Science **318**, 1287 (2007).

[18] See articles in special issue *Dynamics of Electron Transfer Processes at Surfaces*, edited by H. Zacharias, Prog. Surf. Sci. **82**, 161–388 (2007).

[19] See articles in special issue *Dynamics at Solid State Surfaces and Interfaces, Vol. I: Current Developments*, edited by U. Bovensiepen, H. Petek and M. Wolf (Wiley-VCH Verlag GMBH & Co. KgaA, 2010).

[20] S. Neppl, R. Ernstorfer, E. M. Bothschafter, A. L. Cavalieri, D. Menzel, J. V. Barth, F. Krausz, R. Kienberger, and P. Feulner, Phys. Rev. Lett. **109**, 087401 (2012).

[21] M. Bauer, A. Marienfeld, and M. Aeschlimann, Prog. Surf. Sci. **90**, 319 (2015).

[22] P. M. Echenique and J. B. Pendry, J. Phys. C **11**, 2065 (1978).

[23] P. M. Echenique and J. B. Pendry, Prog. Surf. Sci. **32**, 111 (1989).

[24] Th. Fauster and W. Steinmann, in *Electromagnetic Waves: Recent Developments in Research*, edited by P. Halevi (North Holland, Amsterdam 1995), Vol. 2, p. 347.

[25] R. Paniago, R. Matzdorf, G. Meister, and A. Goldmann, Surf. Sci. **336**, 113 (1995).

[26] F. Reinert, G. Nicolay, S. Schmidt, D. Ehm, and S. Hüfner, Phys. Rev. B **63**, 115415 (2001).

[27] E. V. Chulkov, V. M. Silkin, and P. M. Echenique, Surf. Sci. **437**, 330 (1999).

[28] F. J. Himpsel and Th. Fauster, Phys. Rev. Lett. **49**, 1583 (1982).

[29] J. Rogozik, H. Scheidt, V. Dose, K. C. Prince, and A. M. Bradshaw, Surf. Sci. **145**, L481 (1984).

[30] B. Reihl and K. H. Frank, Phys. Rev. B **31**, 8282 (1985).

[31] D. Straub and F. J. Himpsel, Phys. Rev. B **33**, 2256 (1986); and references therein.

[32] R. A. Bartynski and T. Gustafsson, Phys. Rev. B **33**, 6588 (1986); S. Yang, K. Garrison, and R. A. Bartynski, *ibid.* **43**, 2025 (1991).

[33] E. Bertel and U. Bischler, Surf. Sci. **307–309**, 947 (1994); E. Bertel, *ibid.* **331-333**, 1136 (1995).

[34] B. Gumhalter and H. Petek, Surf. Sci. **445**, 195 (2000).

[35] F. El-Shaer and B. Gumhalter, Phys. Rev. Lett. **93**, 236804 (2004).

[36] B. Gumhalter, Phys. Rev. B **72**, 165406 (2005).

[37] P. Lazić, V. M. Silkin, E. V. Chulkov, P. M. Echenique, and B. Gumhalter, Phys. Rev. Lett. **97**, 086801 (2006).

[38] P. Lazić, V. M. Silkin, E. V. Chulkov, P. M. Echenique, and B. Gumhalter, Phys. Rev. B **76**, 045420 (2007).

[39] P. Lazić, D. Aumiler, and B. Gumhalter, Surf. Sci. **603**, 1571 (2009).

[40] F. Aryasetiawan, L. Hedin, and K. Karlsson, Phys. Rev. Lett. **77**, 2268 (1996).

[41] B. Gumhalter, Prog. Surf. Sci. **87**, 163 (2012).

[42] J. Gavoret, P. Nozières, B. Roulet, and M. Combescot, J. Phys. (Paris) **30**, 987 (1969).

[43] S. Doniach, Phys. Rev. B **2**, 3898 (1970).

[44] J. E. Inglesfield, Solid State Commun. **40**, 467 (1975).

[45] W.-D. Schöne and W. Ekardt, Phys. Rev. B **62**, 13464 (2000).

[46] W.-D. Schöne, Int. J. Mod. Phys. B **17**, 5655 (2003).

[47] B. Gumhalter, P. Lazić, and N. Došlić, Phys. Stat. Solidi B **247**, 1907 (2010).

[48] X. Cui, C. Wang, A. Argondizzo, S. Garrett-Roe, B. Gumhalter, and H. Petek, Nat. Phys. **10**, 505 (2014).

[49] Dynamical vertex corrections appearing in the Bethe-Salpether equation pertinent to OA spectra of bulk bands have been approximately solved in the steady-state limit (continuous wave irradiation) in Ref. [50], and implemented in a special computer code in Ref. [51].

[50] A. Marini and R. Del Sole, Phys. Rev. Lett. **91**, 176402 (2003).

[51] A. Marini, C. Hogan, M. Grüning, and D. Varsano, Comp. Phys. Commun. **180**, 1392 (2009).

[52] C. Attaccalite, M. Grüning, and A. Marini, Phys. Rev. B **84**, 245110 (2011).

[53] I. E. Perakis and T. V. Shahbazyan, Surf. Sci. Rep. **40**, 1 (2000).

[54] T. Wolterink, V. M. Axt, and T. Kuhn, Phys. Rev. B **67**, 115311 (2003).

[55] E. V. Chulkov, A. G. Borisov, J. P. Gauyacq, D. Sánchez-Portal, V. M. Silkin, V. P. Zhukov, and P. M. Echenique, Chem. Rev. **106**, 4160 (2006).

[56] S. Mukamel, *Principles of Nonlinear Optical Spectroscopy* (Oxford University Press, New York and Oxford, 1995).

[57] Y. R. Shen, *The Principles of Nonlinear Optics* (Wiley-Interscience, Hoboken, New Jersey, 2003).

[58] A. G. Eguiluz, Phys. Rev. Lett. **51**, 1907 (1983).

[59] A. G. Eguiluz, Phys. Rev. B **31**, 3303 (1985).

[60] V. M. Silkin, J. M. Pitarke, E. V. Chulkov, and P. M. Echenique, Phys. Rev. B **72**, 115435 (2005).

[61] A. Liebsch, Phys. Rev. Lett. **71**, 145 (1993).

[62] A. Liebsch, Phys. Rev. B **57**, 3803 (1998).

[63] H. Ehrenreich and H. R. Philipp, Phys. Rev. **128**, 1622 (1962).

[64] H. U. Yang, J. D'Archangel, M. L. Sundheimer, E. Tucker, G. D. Boreman, and M. B. Raschke, Phys. Rev. B **91**, 235137 (2015); and references therein.

[65] B. N. J. Persson and E. Zaremba, Phys. Rev. B **31**, 1863 (1985).

[66] R. H. Ritchie, Phys. Rev. **106**, 874 (1957).

[67] M. Rocca, Surf. Sci. Rep. **22**, 1 (1995).

[68] M. Rocca, Li Yibing, F. Buatier de Mongeot, and U. Valbusa, Phys. Rev. B **52**, 14947 (1995).

[69] W. Kohn and J. M. Luttinger, Phys. Rev. **98**, 915 (1955).

[70] F. Caruso, H. Lambert, and F. Giustino, Phys. Rev. Lett. **114**, 146404 (2015).

[71] J. Lischner, D. Vigil-Fowler, and S. G. Louie, Phys. Rev. Lett. **110**, 146801 (2013); J. Lischner, G. K. Pálsson, D. Vigil-Fowler, S. Nemsak, J. Avila, M. C. Asensio, C. S. Fadley, and S. G. Louie, Phys. Rev. B **91**, 205113 (2015).

[72] E. R. Fiori and H. M. Pastawski, Chem. Phys. Lett. **420**, 35 (2006).

[73] P. Facchi and S. Pascazio, J. Phys. A Math. Theor. **41**, 493001 (2008).

[74] S. Marion and B. Gumhalter, Phys. Stat. Solidi B **249**, 1218 (2012).

[75] J. Kliewer, R. Berndt, E. V. Chulkov, V. M. Silkin, P. M. Echenique, and S. Crampin, Science **288**, 1399 (2000).

[76] P. M. Echenique, R. Berndt, E. V. Chulkov, Th. Fauster, A. Goldman, and U. Höfer, Surf. Sci. Rep. **52**, 219 (2004).

[77] J. M. Pitarke and M. G. Vergniory, J. Phys.: Condens. Matter **20**, 304207 (2008).

[78] W.-D. Schöne, Prog. Surf. Sci. **82**, 161 (2007).

[79] A similar analysis was carried out for the simpler specular reflection model (SRM) in M. Alducin, R. D. Muiño, and J. I. Juaristi, J. Electron Spectr. Rel. Phenom. **129**, 105 (2003).

[80] D. Lovrić, B. Gumhalter, and K. Wandelt, Surf. Sci. **307–309**, 953 (1994).

[81] D. Lovrić and B. Gumhalter, Surf. Sci. **287/288**, 789 (1993).

[82] D. Lovrić and B. Gumhalter, Phys. Rev. B **38**, 10323 (1988).

[83] See Ch. 8.2. in Ref. [2], and references therein.

[84] G. H. Wannier, Phys. Rev. **52**, 191 (1937).

[85] G. Dresselhaus, J. Phys. Chem. Solids **1**, 14 (1956).

[86] R. J. Elliott, Phys. Rev. **108**, 1384 (1957).

[87] J. J. Hopfield, Phys. Rev. **112**, 1555 (1958).

[88] L. J. Sham and T. M. Rice, Phys. Rev. **144**, 708 (1966).

[89] F. M. Mueller and J. C. Phillips, Phys. Rev. **157**, 600 (1967).

[90] W. Hanke and L. J. Sham, Phys. Rev. B **21**, 4656 (1980).

[91] M. S. Miller and H. D. Drew, J. Phys. F: Met. Phys. **13**, 1885 (1983).

[92] M. Bakshi, G. A. Denton, A. B. Kunz, and C. P. Flynn, J. Phys. F: Met. Phys. **12**, L235 (1982); A. B. Kunz and C. P. Flynn, Phys. Rev. Lett. **50**, 1524 (1983); D. J. Groh, A. B. Kunz, and C. R. Givens, Phys. Rev B **41**, 8037 (1990).

[93] I. Egri, Phys. Rep. **119**, 363 (1985).

[94] Ph. Ghosez, X. Gonze, and R. W. Godby, Phys. Rev. B **56**, 12811 (1997).

[95] G. Onida, L. Reining, and A. Rubio, Rev. Mod. Phys. **74**, 601 (2002).

[96] L. Reining, V. Olevano, A. Rubio, and G. Onida, Phys. Rev. Lett. **88**, 066404 (2002).

[97] Y.-H. Kim and A. Görling, Phys. Rev. Lett. **89**, 096402 (2002).

[98] I. V. Tokatly, R. Stubner, and O. Pankratov, Phys. Rev. B **65**, 113107 (2002); R. Stubner, I. V. Tokatly, and O. Pankratov, *ibid.* **70**, 245119 (2004).

[99] F. Sottile, V. Olevano, and L. Reining, Phys. Rev. Lett. **91**, 056402 (2003).

[100] A. Marini, R. Del Sole, and A. Rubio, Phys. Rev. Lett. **91**, 256402 (2003).

[101] S. Botti, F. Sottile, N. Vast, V. Olevano, L. Reining, H.-C. Weissker, A. Rubio, G. Onida, R. Del Sole, and R. W. Godby, Phys. Rev. B **69**, 155112 (2004).

[102] F. Bruneval, F. Sottile, V. Olevano, and L. Reining, J. Chem. Phys. **124**, 144113 (2006).

[103] O. Betbeder-Matibet and M. Combescot, Eur. Phys. J. B **22**, 17 (2001).

[104] M. Combescot, O. Betbeder-Matibet, and B. Roulet, Europhys. Lett. **55**, 717 (2002).

[105] V. Turkowski, A. Leonardo, and C. A. Ullrich, Phys. Rev. B **79**, 233201 (2009).

[106] M. Molotskii, Appl. Phys. Lett. **95**, 084103 (2009).

[107] V. U. Nazarov and G. Vignale, Phys. Rev. Lett. **107**, 216402 (2011).

[108] Z.-H. Yang and C. A. Ullrich, Phys. Rev. B **87**, 195204 (2013).

[109] K. Miwa, M. Sakaue, B. Gumhalter, and H. Kasai, J. Phys.: Condens. Matter **26**, 222001 (2014).

[110] A. Chernikov, T. C. Berkelbach, H. M. Hill, A. Rigosi, Y. Li, O. B. Aslan, D. R. Reichman, M. S. Hybertsen, and T. F. Heinz, Phys. Rev. Lett. **113**, 076802 (2014).

[111] J.-H. Choi, P. Cui, H. Lan, and Z. Zhang, Phys. Rev. Lett. **115**, 066403 (2015).

[112] S. Ono, Phys. Rev. B **92**, 125101 (2015).

[113] C. C. Marston and G. Balint-Kurti, J. Chem. Phys. **91**, 3571 (1989); J. Stare and G. Balint-Kurti, *ibid.* **107**, 7204 (2003); I. Matanović and N. Došlić, *ibid.* **109**, 4185 (2005); I. Matanović, N. Došlić, and O. Kuehn, *ibid.* **127**, 014309 (2007).

[114] G. H. Golub and C. F. Loan, *Matrix Computations* (The Johns Hopkins University Press, Baltimore, MD, 1985).

[115] D. Sorensen, *Tutorial: Implicitly Restarted Arnoldi/Lanczos Methods for Large Scale EigenValue Calculations* (Rice University, Houston, TX, 1995).

[116] An analogous decomposition of excitonic energies but for statically screened 2D isotropic excitonic interaction in quantum wells was presented in Ref. [110].

[117] G. D. Mahan, Surf. Sci. **606**, 1542 (2012).

[118] M. Born and V. Fock, Z. Physik A **51**, 165 (1928).

[119] L. I. Schiff, *Quantum Mechanics* (McGraw-Hill Book Company, New York, 1968), p. 289.

[120] L. D. Landau and E. M. Lifshitz, *Quantum Mechanics* (Addison-Wesley, Reading, Massachusets 1958), p. 261.

[121] C. Zener, Proc. Roy. Soc. A **137**, 696 (1932).

[122] See Supplemental Material at http://link.aps.org/supplemental/10.1103/PhysRevB.92.155405 for the development of theoretical descriptions of the invoked Landau-Zener transitions and their incorporation into the expressions for 3PP yields.

[123] J.-C. Deinert, D. Wegkamp, M. Meyer, C. Richter, M. Wolf, and J. Stähler, Phys. Rev. Lett. **113**, 057602 (2014).

[124] H. Ueba and B. Gumhalter, Prog. Surf. Sci. **82**, 193 (2007).

[125] T. F. O'Malley, Adv. At. Mol. Phys. **7**, 223 (1971), and references therein.

[126] Similar equations but in the coordinate space were considered by: L. J. Fernandez-Alcazar and H. M. Pastawski, Eur. Phys. Lett. **105**, 17005 (2014).

[127] L. B'anyai, D. B. Tran Thoai, E. Reitsamer, H. Haug, D. Steinbach, M. U. Wehner, M. Wegener, T. Marscher, and W. Stolz, Phys. Rev. Lett. **75**, 2188 (1995).

[128] Q. T. Vu, H. Haug, and L. V. Keldysh, Solid State Comm. **115**, 63 (2000).

[129] C. Cohen-Tannoudji, J. Dupont-Roc, and G. Grynberg, *Photons and Atoms, Introduction to Quantum Electrodynamics* (Wiley Professional Paperbacks, New York, 1997), p. 324.

[130] N. W. Ashcroft and W. L. Schaich, in *Electronic Density of States*, 3rd Materials Research Symposium (Gaithersburg, Maryland, 3-6 Nov. 1969), National Bureau of Standards Special Publication **323**, 129 (1971); W. L. Schaich and N. W. Ashcroft, Phys. Rev. B **3**, 2452 (1971).

[131] See Sec. 3 of the Supplementary Information in Ref. [48].